DETECTION AND CLASSIFICATION OF MELANOMA USING DENSE CONVOLUTIONAL NEURAL NETWORK

2022
MASTER THESIS
COMPUTER ENGINEERING

Mohammed Yousif ARABI

Thesis Advisor
Assist. Prof. Dr. Adnan Saher M. AL-AJEELI

DETECTION AND CLASSIFICATION OF MELANOMA USING A DENSE CONVOLUTIONAL NEURAL NETWORK

Mohammed Yousif Arabi AL-KHUZAIE

T.C.
Karabuk University
Institute of Graduate Programs
Department of Computer Engineering
Prepared as
Master Thesis

Thesis Advisor

Assist. Prof. Dr. Adnan Saher M. AL-AJEELI

KARABUK

July 2022

I certify that in my opinion the thesis submitted by Mohammed Yousif Arabi AL-KHUZAIE titled "DETECTION AND CLASSIFICATION OF MELANOMA USING DENSE CONVOLUTIONAL NEURAL NETWORK" is fully adequate in scope and in quality as a thesis for the degree of Master of Computer Engineering.

Assist. Prof. Dr. Adnan Saher M. AL-AJEELI ……...
Thesis Advisor, Department of Computer Engineering

This thesis is accepted by the examining committee with a unanimous vote in the Department of Computer Engineering as a Master of Science thesis. July 21,2022

Examining Committee Members (Institutions) Signature

Chairman: Prof. Dr. Fatih Vehbi ÇELEBI (AYBU) ……..

Member: Assist. Prof. Dr. Caner ÖZCAN (KBU) ……

Member: Assist. Prof. Dr. Adnan Saher M. AL-AJEELI (KBU) …….....

The degree of Master of Computer Engineering by the thesis submitted is approved by the Administrative Board of the Institute of Graduate Programs, Karabuk University.

Prof. Dr. Hasan SOLMAZ .....
Director of the Institute of Graduate Programs

"I declare that all the information within this thesis has been gathered and presented in accordance with academic regulations and ethical principles and I have according to the requirements of these regulations and principles cited all those which do not originate in this work as well."

Mohammed Yousif Arabi AL-KHUZAIE

ABSTRACT

M. Sc. Thesis

DETECTION AND CLASSIFICATION OF MELANOMA USING A DENSE CONVOLUTIONAL NEURAL NETWORK

Mohammed Yousif Arabi AL-KHUZAIE

Karabuk University
Institute of Graduate Programs
The Department of Computer Engineering

Thesis Advisor:
Assist. Prof. Dr. Adnan Saher M. AL-AJEELI
July 2022, 73 pages

Melanoma is the most dangerous kind of skin inflammation. Despite its rarity, this condition is fatal, and diagnosing it using standard methods is difficult due to the high level of skill and medical equipment required, as well as the length of time required for diagnosis, necessitating the development of a new diagnostic approach.

Early identification of skin cancer is a critical step that can aid in the delivery and elimination of effective treatment. As a result, effective early detection procedures for skin cancer are in high demand in health institutions and medical centers, and they require ongoing development to provide high-quality and accurate diagnostic results.

Deep learning's main goal is to identify an effective feature that detects the melanoma pathway automatically, and there are serious attempts to develop new learning models developing imaging systems and technologies that can deal with traditional images so that high-spectrum images can be distinguished from others.

This paper uses a dense convolutional neural network (Dense-CNN) model for melanoma diagnosis. The proposed model was applied to eight datasets: the HAM10000 dataset, ISIC 2019, DermQuest-DermIS, ISIC 2017, ISIC 2016, MED-NODE, PH2 dataset, and DermNet. All of these datasets are for images of skin lesions obtained through dermatoscopy. Our results were compared with those of other studies. When applied to the eight datasets, the proposed model achieved high diagnostic rates in terms of accuracy, sensitivity, specificity, and precision.

Keywords: Melanoma, Dermoscopy, Dense-Convolutional neural networks, Deep learning, DermQuest-DermIS.
Science code: 92431

ÖZET

Yüksek Lisans Tezi

YOĞUN BİR KONVOLÜSYONEL SİNİR AĞI KULLANARAK MELANOMUN TESPİTİ VE SINIFLANDIRILMASIGELİŞTİRİLMESİ

Mohammed Yousif Arabi AL-KHUZAIE

Karabük Üniversitesi
Lisansüstü Eğitim Enstitüsü
Bilgisayar Mühendisliği Anabilim Dalı

Tez Danışmanı:
Dr. Öğr. Üyesi Adnan Saher M. AL-AJEELI
Temmuz 2022, 73 sayfa

Melanom, cilt iltihabının en tehlikeli türüdür. Nadir olmasına rağmen, bu durum ölümcüldür, ve standart yöntemlerle teşhis etmek zordur, çünkü yüksek düzeyde beceri ve gerekli tıbbi ekipman gerekmektedir. Tanı için gerekli sürenin yanı sıra yeni bir teşhis yaklaşımının geliştirilmesini gerekli kılmaktadır. Sağlık açısından erken dönemde, sağlık bakımına yönelik incelemeler konusunda çok önemli bir adımdır. Sonuç olarak, cilt kanseri için etkili erken teşhis prosedürleri, sağlık kurumlarında ve tıp merkezlerinde yüksek talep görmektedir ve yüksek kaliteli ve doğru teşhis sonuçları sağlamak için sürekli geliştirmeye ihtiyaç duyarlar. Derin

öğrenmenin ana hedefi, melanom yolunu algılayan etkili bir özelliği otomatik olarak belirlemektir ve yüksek spektrumlu görüntülerin diğerlerinden ayırt edilebilmesi için geleneksel görüntülerle başa çıkabilecek görüntüleme sistemleri ve teknolojileri geliştirerek yeni öğrenme modelleri geliştirmeye yönelik ciddi girişimler vardır.

Bu tez çalışmasında, melanom teşhisi için yoğun bir evrişimli sinir ağı (Dense-CNN) modeli tasarlanmıştır. Önerilen model sekiz veri kümesine uygulandı: HAM10000 veri kümesi, ISIC 2019, DermQuest-DermIS, ISIC 2017, ISIC 2016, MED-NODE, PH2 veri kümesi ve DermNet. Bu veri setlerinin tümü, Dermoskopi ile elde edilen deri lezyonlarının görüntüleri içindir. Sonuçlarımız diğer çalışmaların sonuçlarıyla karşılaştırıldı. Sekiz veri kümesine uygulandığında, önerilen model doğruluk, duyarlılık, özgüllük ve kesinlik açısından yüksek tanı oranları elde etti.

Anahtar Kelimeler: Melanom, Dermoskopi, Yoğun-Evrişimli sinir ağları, Derin öğrenme, DermQuest-DermIS.
Bilim Kodu: 92431

ACKNOWLEDGMENT

I owe thanks and praise to God first and foremost for this success and facilitation as I bow to my beloved parents. My dear father gave me the most valuable things to make me a man of honor. My beloved mother is good at engineering my heart with her prayers. To my family that I grew up in and its extension gives me pride and honor. I owe a special thanks to my thesis supervisor, Assist. Prof. Dr. Adnan Saher M. AL-AJEELI who spared no effort in providing unlimited advice and guidance until the completion of this thesis to the fullest.

I also extend my gratitude to Karabuk University, including the wonderful professors and colleagues who accompanied us throughout our academic journey, especially Dr. Osamah Taher.

I dedicate this thesis to my beloved country, Iraq. And to the beautiful Turkey, which embraced this scientific experience and contributed to providing all possibilities for graduating in this distinguished way.

LIST OF CONTENTS

Page

APPROVAL.……...……ii

ABSTRACT.....iv

ÖZET.....vi

ACKNOWLEDGMENT.....viii

LIST OF FIGURES xiii

ABBREVIATIONS xvi

PART 1 1

INTRODUCTION 1

1.1. OVERVIEW..... 1
1.2. CLASSES OF SKIN CANCER 1
1.2.1. Melanoma 1
1.2.2. Melanoma Nevus 2
1.2.3. Basal Cell Carcinoma (BCC)..... 2
1.2.4. Squamous Cell Carcinoma 2
1.3. TRADITIONAL DIAGNOSIS OF MELANOMA..... 3
1.3.1. CAD-Based Diagnosis..... 3
1.3.2. ABCD Rule..... 3
1.3.3. Pattern analysis 5
1.3.4. Menzies Method 5
1.3.5. 7-Point Checklist..... 5
1.4. MOTIVATION..... 5
1.5. PROBLEM STATEMENT..... 6
1.6. STUDY OBJECTIVES..... 7
1.7. CONTRIBUTIONS 7

Page

PART 2 8

LITERATURE REVIEW 8

PART 3 15

CONVOLUTIONAL NEURAL NETWORK 15

3.1. MACHINE LEARNING 15

3.1.1. Supervised Learning 15

3.1.2. Unsupervised Learning 16

3.1.3. Semi-Supervised Learning 16

3.1.4. Reinforcement Learning 16

3.2. DEEP LEARNING 17

3.2.1. Convolutional Neural Network 18

3.2.1.1. Convolutional Layer2 18

3.2.1.2. Pooling Layer 22

3.2.1.3. Fully Connvolutonal Layer (FC) 23

3.2.1.4. Dropout layer 23

3.2.1.5. Batch Normalization 24

3.3. DENSE LAYER 24

3.4. PERFORMANCE METRICS 25

3.4.1. Accuracy 25

3.4.2. Sensitivity 26

3.4.3. Specificity 26

3.4.4. Positive Predictive Value (PPV) 26

3.4.5. NegativePredictive Value (NPV) 27

3.4.6. Precision (PRE) 27

3.4.7. F1-Score 27

3.4.8. Reciever Operating Curve (ROC) 27

PART 4 28

METHODOLOGY 28

Page

4.1. DATA COLLECTION 28
4.2. DATA PREPARATION 29
4.2.1. Platform Used 29
4.2.2. Initializing Libraries 29
4.2.3. Data Splitting 31
4.2.4. Data Augmentation 32
4.2.5. Data Allocation 33
4.2.5.1. Classes-Based Distribution 34
4.2.5.2. Gender-Based Distribution 35
4.2.5.3. Age-Based Distribution 36
4.3. PREPROCESSING 37
4.3.1. Data Cleaning 38
4.3.2. Data Normalization 38
4.4. OVERSAMPLING 38
4.5. OBSTACLES 39
4.6. SYSTEM IMPLEMENTATION 40
4.6.1. Proposed Model 40
4.6.2. Proposed Dense Layer Architecture 42
4.6.3. Model Training 45
4.6.4. Model Testing 46

PART 5 48

RESULT AND DISCUSSION 48

5.1. TEST RESULTS OF DENSE ON HAM10000 DATASET 49
5.2. TEST RESULTS OF DENSE ON THE ISIC 2019 DATASET 50
5.3. TEST RESULTS OF DENSE ON THE DERMIS DERMQUEST 52
5.4. TEST RESULTS OF DENSE ON THE ISIC 2017 DATASET 53
5.5. TEST RESULTS OF DENSE ON THE ISIC 2016 DATASET 54
5.6. TEST RESULTS OF DENSE ON THE MED-NODE DATASET 56
5.7. TEST RESULTS OF DENSE ON THE PH² DATASET 57
5.8. TEST RESULTS OF DENSE ON THE DERMNET DATASET 58

Page

5.9. COMPARING WITH RELATED WORKS 60

PART 6 63

CONCLUSION 63

REFERENCES 64

RESUME 73

LIST OF FIGURES

Page

Figure 1.1. Displays the various stages of skin cancer 1
Figure 1.2. Classifications of skin cancer 4
Figure 3.1. A typical illustration of the convolutional neural network 18
Figure 3.2. Display activation formats 20
Figure 3.4. Display fully connected layers. 23
Figure 3.5. Five-layer dense block using all previous feature maps as input. 24
Figure 4.1. For example, standardization and splitting data 31
Figure 4.2. For example, standardization and splitting data, after reshaping and resizing 32
Figure 4.3. Example of melanoma Images after data augmentation 33
Figure 4.4. Shows the distribution of skin cancer classes 34
Figure 4.5. Frequency distribution of classes 34
Figure 4.6. Patient gender distribution 35
Figure 4.7. Example for standardization and splitting data 36
Figure 4.8. Histogram of the patient's age 37
Figure 4.9. Random Oversampling 39
Figure 4.10. The model that was proposed and designed by us 42
Figure 4.11. Sketch of the melanoma detection model 44
Figure 4.12. Flowchart of block of proposed system 45
Figure 4.13. Flowchart of Testing-Training model 47
Figure 5.1. Plots (A and B) show the performance results of the Dense-CNN model using the HAM 10000 dataset. 50
Figure 5.2. Confusion matrix for Dense-CNN with 50 epochs-9387 testing images of HAM10000 dataset. 50
Figure 5.3. Plots (A and B) show the performance results of the Dense-CNN model using the ISIC 2019 dataset. 51

Page

Figure 5.4. Confusion matrix for Dense-CNN model with 50 epochs-8116 testing images of ISIC 2019 dataset. 51

Figure 5.5. Plots (A and B) show the performance results of the Dense-CNN model using the DermIS-DermQuest dataset. 52

Figure 5.6. Confusion matrix for Dense-CNN model with 50 epochs- 6156 testing images of DermIS-DermQuest dataset. 53

Figure 5.7. Plots (A and B) show the performance results of the Dense-CNN model on the ISIC 2017 dataset. 54

Figure 5.8. Confusion matrix for Dense-CNN with 50 epochs- 5598 testing images of ISIC 2017 dataset. 54

Figure 5.9. Plots (A and B) show the performance results of the Dense-CNN model on the ISIC 2016 dataset. 55

Figure 5.10 Confusion matrix for Dense-CNN with 50 epochs- 5850 testing images of ISIC 2016 dataset. 55

Figure 5.11. Plots (A and B) show the performance results of the Dense-CNN model on the MED-NODE dataset. 56

Figure 5.12. Confusion matrix for Dense-CNN with50 epochs- 4052 testing images of MED-NODE dataset. 57

Figure 5.13. Plots (A and B) show the performance results of the Dense-CNN model on the PH² dataset. 58

Figure 5.14. Confusion matrix for Dense-CNN with 50 epochs-170 testing images of PH² dataset. 58

Figure 5.15. Plots (A and B) show the performance results of the Dense-CNN model on the DermNet dataset. 59

Figure 5.16. Confusion matrix for Dense-CNN with50 epochs-518 testing images of DermNet dataset. 59

Figure 5.17. Comparison of the performance of the Dense-CNN model on eight datasets. 60

Figure 5.18. A comparison of the prediction accuracy between our proposed model (highest rate with ISIC 2019) and other existing studies. 62

LIST OF TABLES

Page

Table 2.1. Review of related literature 13
Table 4.1. Displays number of images for each dataset 29
Table 4.2. Dense sequential model 41
Table 5.1. Distribution of the images after data augmentation 49
Table 5.2. Describes the performance of Dense-CNN on the HAM10015 dataset. 49
Table 5.3. Describes the performance of Dense-CNN on the ISIC 2019 dataset. ... 51
Table 5.4. Describes the performance of Dense-CNN on the DermIS-DermQuest dataset. 52
Table 5.5. Describes the performance of Dense-CNN on the ISIC 2017 dataset. ... 53
Table 5.6. Describes the performance of Dense-CNN on the ISIC 2016 dataset. 55
Table 5.7. Describes the performance of Dense-CNN on the MED-NODE dataset. 56
Table 5.8. Describes the performance of Dense-CNN on the PH^2 dataset. 57
Table 5.9. Describes the performance of Dense-CNN on the DermNet dataset. 59
Table 5.10. Comparing our experimental results with other exciting works and our proposed model (highest rate with ISIC 2019). 61

ABBREVIATIONS

ABCD:	Asymmetry, Border, Color Variation, and Diameter
ANN:	Artificial neural networks
AUC:	Area under the characteristic curve
ACC:	Accuracy
CAD:	Computer-aided diagnosis
CMLD:	CNN malignant lesion detection
CNN's:	Convolutional neural networks
CSC-Mel:	Classifier skin cancer-Melanoma
DNN:	Deep neural network
DNA:	Deoxyribonucleic acid
ELM:	Extreme learning machine
FP:	False positives
FN:	False negatives
FCV:	Fold cross validation
GANs:	Generative Adversarial Networks
GLCM:	Gray level co-occurrence matrix
GWO:	Gray wolf optimization
ISIC:	International Skin Imaging Collaboration
LIME:	Local Interpretable Model-agnostic Explanations
K-NN:	K-Nearest neighbor
RBF:	Radial basis function
ReLU:	A rectified linear unit
NHIS:	The National Health Interview Survey

ROC: Receiver operating characteristic curve

SURF: Speeded Up Robust Features

SVM: Support Vector Machine

TP: True positives

TN: True negatives

WHO: World Health Organization

PART 1

INTRODUCTION

1.1. OVERVIEW

Melanoma, the most serious form of skin cancer, is distinguished by the presence of melanocytes. Skin illnesses are, without a doubt, common around the globe. Squamous cell carcinoma is a malignancy that affects a large percentage of people in the United States and elsewhere. According to statistics [1,2], One out of every 39 healthy adults suffered an injury in 2010. The World Health Organization (WHO) estimates that 1,200,000 cases of non-malignant melanoma will be diagnosed in 2020. It's worth noting that melanoma is ranked fourth among the diseases that have the greatest economic impact [1,3]. Despite these diseases' rarity, most people who develop malignant skin cancer die within two years [4].

Melanocytes are pigment cells that generate melanin, protecting our bodies from damaging ultraviolet rays. Melanocytes are responsible for the pigmentation of skin color since they produce melanin [5]. Mutations in the deoxyribonucleic acid (DNA) genetic strand of skin cells cause the disease to develop. Excessive exposure to ultraviolet rays emitted by sunlight causes genetic changes, resulting in an aberrant and excessive proliferation of cancerous cells [6-7].

Deep learning has become widely used in numerous sectors, including medicine. Over the previous two decades, it has evolved into a sophisticated approach for recognizing and distinguishing skin disorders, particularly melanoma. With the help of dermatoscopy and digital computer images, various deep learning network methods are used, with color images being used primarily in developing artificial intelligence algorithms and access to image data in big sets.

A considerable quantity of data and information is required to train and retrieve pictures from CNN networks. Both in training and in athletics, this requires a lot of time and effort [5,8] Dermatological disorders and their categorization may overlap or be classified incorrectly due to the complexity of the differentiation process. Using a variety of filters, CNN networks evaluate images' edges and lines to generate enormous amounts of data at the network's early and deep layers, where the networks can better describe those edges and contrast.

1.2. CLASSES OF SKIN CANCER

A skin lesion is an uncontrolled mass of skin compared to the skin around it [9]. There are many different sorts of skin lesions and diseases that range from simple inflammatory conditions like warts to more serious issues like skin malignancies. Basal, squamous, and melanomas are the three major types of skin cancer [10]. Various methods and textures are used to detect a variety of skin cancers. Figure (1.1) depicts the various stages of skin cancer.

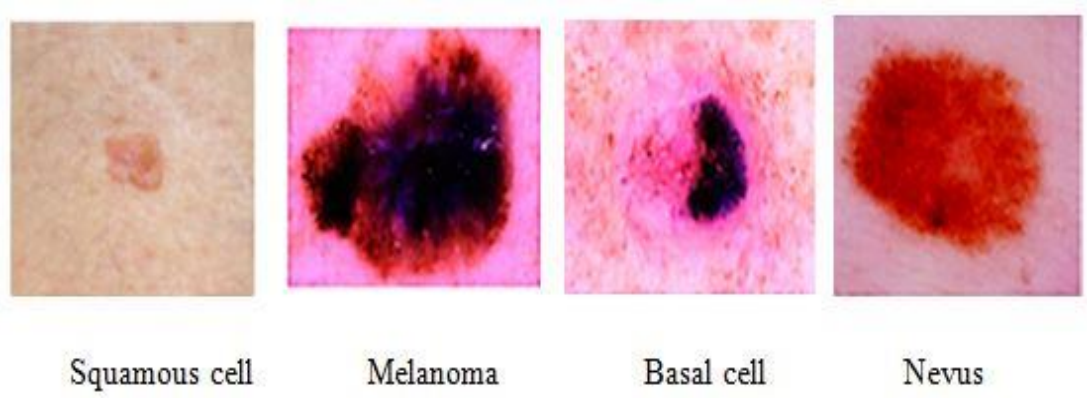

Figure 1.1. Displays the various stages of skin cancer[8].

1.2.1. Melanoma

The first onset of skin cancer starts in the melanocytes (the cells responsible for pigmentation). It can start in the eyes, intestines, or other body regions containing pigmented tissue, but it is more frequent in the skin [12]. Five distinct features

distinguish melanomas. The acronym "ABCDE" aids memorization of pest asymmetry, boundaries, color, dimension, and evolution.

1.2.2. Melanoma Nevus

A mole is a form of melanocytic neoplasm that includes nevus cells. They are frequently congenital or manifest themselves during childhood and adolescence [13]. Although most moles are just plain brown spots, they can have a set of attributes: Surface and color: Moles come in various colors, including brown, tan, black, red, blue, and pink. They can be flat, elevated, wrinkled, or smooth. They may have hair hanging out of them.

1.2.3. Basal Cell Carcinoma (BCC)

While BCC can show in various ways, the most typical sign is a raised, whitish lump that might be inflammatory or asymptomatic. In cancer, venules (telangiectatic vessels) are occasionally visible [13]. Light skin on the head, neck, chest, and shoulders is the most common site for this malignancy. The middle face is a high-risk location for cancer recurrence following initial therapy [14].

1.2.4. Squamous Cell Carcinoma

In areas of the skin that are often exposed to the sun, such as the ears, the lower lip, and the backs of the hands, CSCs are more prevalent. CSCs appear red, scaly, thickened areas, open wounds, or ulcerated skin [14].

1.3. TRADITIONAL DIAGNOSIS OF MELANOMA

1.3.1. CAD-Based Diagnosis

CAD has become a mainstay in traditional oncological diagnostic methods. These systems use digital images to help interpret medical images such as x-rays, diagnostic radiology, ultrasound, and others [15,16]. There is an important role in applying the CAD system in the classification of skin cancer. The doctor depends on the results of the analysis [17]. Therefore, computerized medical images have become a second opinion in detecting lesions and arriving at the correct diagnosis. In the CAD system, there are five fundamental processes that we might use to classify images:

1. Image preprocessing: To reduce image noise and imperfections while increasing the contrast.
2. Segmentation: It is the division of an image into regions with defined qualities.
3. As part of the dimensionality reduction process, a vast quantity of raw data is broken down and reduced into smaller, more manageable pieces. By finding variables and merging them into features, feature extraction aids in extracting the best features from these massive data sets, effectively lowering the amount of data.
4. Classification: Using a suitable classification algorithm that compares image patterns to target patterns, this stage categorizes identified items into predetermined classes.
5. Evaluation of performance: There are various methods for evaluating performance, including the receiver operating characteristic curve (ROC).

1.3.2. ABCD Rule

The ABCD rule, sometimes known as the ABCDE rule, is a set of diagnostic criteria for skin cancer (Asymmetry, Border, Color, Diameter, and Evolving) [11]. When photographs of skin tissue are available, these characteristics may assist differentiate between benign and malignant melanoma. (A) Asymmetry: The input image is divided along a perpendicular axis to reduce asymmetry. If the asymmetry occurs

along the axes, a score of 2 is given; otherwise, a score of 1 is given. zero for no asymmetry. (B) Border: Check for sudden and abrupt changes. A sharp cutoff scores 1, whereas a gradual cutoff scores 0. (C) Color: Cancer detection utilises the colours black, brown, white, red, and pink. Counting the hues. (D) Diameter: The circumference of the lesion is carefully measured. A tumour having a diameter more than or equal to 6 millimetres is referred to be a melanoma [18-19]. The block diagram in Figure represents each strategy covered in this section (1.2).

$$S_{abcd} = \sum_{i=1}^{4} WiPi \tag{1.1}$$

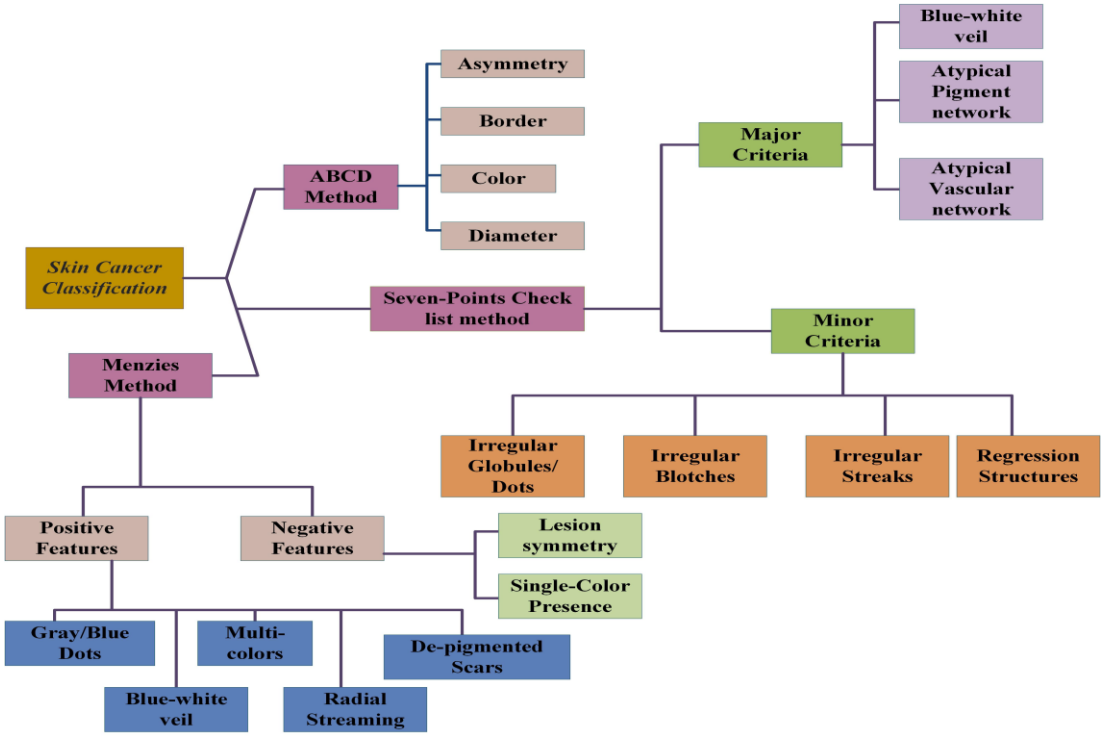

Figure 1.2. Classifications of skin cancer[11].

1.3.3. Pattern analysis

The Pattern analysis (PA) technique is a progressive algorithm for diagnosing pigmented skin lesions with melanin, substantial blood pigmentation (as in noncrystalline blood or red clods), or discolored keratin. This method was utilized for more than 20 years. It is among the most reliable methods available. There has been no procedure that has been proven to be more effective, but there were no different methods, and the vocabulary of dermatoscopy developed with a plethora of ill-defined or ambiguous metaphorical terminology, many of which had predetermined diagnostic meanings [6], [20].

1.3.4. Menzies Method

The Menzies technique is a computer algorithm that recognizes two negative and nine positive characteristics of dermatoscopy. To be classified as melanoma, the lesion must not have any of the two negative criteria and at least one of the nine positive aspects [21].

1.3.5. 7-Point Checklist

The "7-point checklist" is a different diagnostic strategy based on a streamlined pattern analysis with seven standard parameters [22]. The seven factors are divided into major and minor categories based on their clinical weight, with the diagnosis of melanoma being indicated when at least two factors (one major and one small criterion) are met. Ultimately, a score is determined by adding the point values depending on the existence of each criterion, and the lesion is categorized as melanoma if the score is larger than three [23].

1.4. MOTIVATION

Because of the importance of this topic, numerous studies and research have been conducted in the past, and many students and researchers are continuously studying it. Despite the vast number of studies on the issue of skin disease detection and categorization in general and melanoma, there is still a gap in this area that researchers

must fill. Most of the past research on this subject has concentrated on one component of the images, characterized by white skin, although multiple relevant factors may have had a part in the discovery. Not all skin lesions were recognized in most prior research studies, and segmentation and categorizing of medical images is one of the most significant methods for determining the location of a skin condition.

1.5. PROBLEM STATEMENT

Whereas deep learning can dynamically extract and classify features and beat classic existing algorithms, [24] the key obstacle is data availability and legality. Machine learning works best when there is a lot of data, which is tough to come by in the medical field. The two main roadblocks are data availability concerns and the need to resolve legal issues connected to preserving patient privacy. They are training an efficient machine. The learning model is hampered by data scarcity, privacy, dependability, and other legal difficulties.

Several data enrichment techniques are available to tackle the issues of small datasets. This augmentation strategy entails several techniques for increasing the volume and quantity of data to make deep learning methods easier to train.

Several ways could be used to supplement the samples. One of these ways is through traditional medical imaging data augmentation approaches involving transformations like resizing [25], rotation, and translation.

These changes are effective up to a point, but after that, they can limit deep learning's ability to generalize to new data. Another way is by using classic augmentation procedures in small amounts and combining them with different enhancement techniques.

1.6. STUDY OBJECTIVES

This thesis aims to create a model that uses deep learning algorithms to detect and classify melanoma. Several significant duties must be mentioned to attain the thesis's goal:

1. Establish an efficient learning system that can detect and evaluate skin lesions' photos to determine whether they are malignant or benign.
2. Affirmation that our results are more accurate in detecting skin cancer than others have done in previous research, as well as to ensure that this differentiation is more dependable than what is obtained by doctors and specialists in histology departments.
3. Using the eight most commonly available, publicly available datasets on skin lesions

1.7. CONTRIBUTIONS

This thesis has many high-level features that allow them to get precise information and make the system easy to use, giving users many credibilities and increasing their trust in the system. We wanted to ensure that each feature had logical information in the system design, making transferring the features to the dermatologist easier. On the other hand, we were eager to develop a decision-support system for dermatologists and other healthcare professionals who found the dermatoscopy technique challenging. The technology has undergone image analysis through a conventional camera for ease of usage. The features are also built to work in specific circumstances, so you can get unconstrained images and modify the resolution quality and lighting conditions.

PART 2

LITERATURE REVIEW

The healthcare industry is continuously seeking for new ideas and strategies to enhance since it is so vital and directly related to human health. Artificial intelligence (AI) technology in healthcare, specifically deep learning (DL) and data mining, has been the focus of several research. Artificial Intelligence (AI) technologies have lately had a lot of success in the healthcare area when it comes to extracting information from health data. For a long time, data mining methods have been utilised to identify and predict illness.

Studies on image classification and differentiation have been summarised and described in this area. New research that employed deep learning algorithms to identify and categorise pictures of skin lesions help to do this. Clinicians can more easily and accurately detect and evaluate different types of skin lesions with the help of precise categorization and differentiation of skin lesions.

The outcomes from these studies, although promising, cannot be compared to the ones from our own research. This is due to the fact that earlier research only utilised one or two data sets, while we used eight and applied our suggested model to them.

Edgar Omar Molina-Molina [26] devised a technique for diagnosing a skin lesion based on 100 characteristics collected from the Densenet-201. To make this strategy work, three one-dimensional fractal subscriptions of colour pictures are utilised. The researchers used a digital computer and a KNN classifier with two support vectors to do clustering. They used the number of polylines to map the diagnostic outputs of the images. Accuracy of 97%, sensitivity of 66.45%, and specificity of 97% were achieved using the archived dataset (ISIC)-2019.

Using the transfer learning approach, A Gong et al. [27] were able to train CNNs and GANs simultaneously. Individual feature sets were mined for feature extraction and classification, and dermatoscopy images were analysed as a whole. CNN's performance with the ISIC 2018 dataset was evaluated against that of other frames and models in order to identify various types of pictures. The approach has a 92.4 percent accuracy rate, a 48.3% sensitivity rate, and a 97.7% specificity rate.

It has been suggested that segmentation be used in conjunction with computer-aided CNNs, such as those developed by Doaa A. Shoaib and colleagues [28] to help diagnose skin lesions in images. The SVM vector was used to generate a grid for feature extraction. Three hundred and thirty-seven different images of skin lesions were culled from two sets of data. DermQuest and an open-source internet dermatology dataset make up the first two datasets. There is a 94% accuracy, 100% sensitivity and 88% specificity in the suggested model, which is superior than existing models in the field.

The (ISIC) 2018 dataset was used to train a multi-configuration CNN neural network by Mohamed, Abeer et al. [29] In order to diagnose melanomas, they categorised photos. According to the suggested model's prediction accuracy of 97%, the network has 14 layers.

An alternative CNN model known as CMLD was used by Soumen Mukherjee et al. [30] For this study, two distinct sets of Dermofit and MedNODE imaging data were analysed, and then integrated. Prediction rates of 90.58% and 90.14% may be achieved when the two groups are utilised individually with 10-fold growing amounts of data, whereas the accuracy decreases to 83.07% when the two groups are combined.

AlexNet was used to train the ISIC 2018 dataset by Sertan Kaymak et al [31]. Images of the skin mass were used to identify characteristics and categorise the pictures for this diagnosis. When the data set was partitioned, three models were built to represent the pigmented and non-pigmented layers. The second model was more accurate, with an accuracy of 84.4 percent, a sensitivity of 84.7%, and a specificity of 83.8%, in distinguishing benign from malignant melanoma.

Based on the 1279 pictures from the ISIC archive collection, Lopez, Adria Romero et al. [32] proposed constructing VGGNet, a convolutional neural network, for classification and feature extraction. There were three classification methods used, all of which were based on transfer learning and network training. The model was put to use in three different ways, with the third method proving to be the most effective. 78.66% of the data was sensitive, and 81.330% of the data was accurate.

.

The CNN-New Regulaizer model was proposed by Albahar and Marwan Ali [33] for constructing a novel prediction model and extracting features. With the use of ISIC data, we were able to categorise skin lesions into two distinct groups. Benign carcinomas are the first kind, whereas malignant carcinomas are the second. In terms of AUC-ROC prediction accuracy, this technique is superior than several existing methods. Model accuracy, sensitivity, and specificity are all over 94% in the suggested model.

The dermatoscopy pictures were cleaned up by NudratNida et al. [34] to make the diagnosis easier. Maps and feature extraction for model learning were performed using the melanoma area's measurements. The extreme learning machine (ELM) was used with the two datasets (ISIC-2016 and ISIC-2017). The ISIC-2017 dataset has a 93 % accuracy rate compared to the ISIC-2016 dataset's 85 % accuracy rate.

It is suggested that to create an ANN for picture classification, the authors Kanimozhi, T., and A. Murthi [35] use a set of 31 data points from images taken by hospitalised melanoma patients and back propagation and training on that data. The ABCD method was used to identify the colour, diameter, border, and consistency of the tissue. When it came to solving this problem, we used MATLAB. In terms of accuracy and classification efficiency, the model performed brilliantly, with a 96% accuracy rate.

According to Dalila and colleagues [36] an ant colony-based segmentation approach might be used to detect various skin lesions criteria, such as geometric features and relative colours. A total of 172 dermatoscopy photos were classified using KNN and

neural network methods. Using 12 skin lesion features, the algorithm was able to accurately predict the outcome of a test.

Accuracy was an important goal for Sugiarti and colleagues [37]. An ANN-based classification approach is used to extract texture-based traits. MLP (Multilayer Perceptron) was used for both training and testing in this project for each pair of benign and malignant melanoma photographs, four sets of 23 shots were used with an accuracy of 80% and 88.88%.

For extracting characteristics from skin photographs, SharminMajumder et al. [38] developed an ANN model based on the ABCD rule. The PH 2 dataset was trained using this dataset. To get rid of unwanted hair from photos, they turned to the Dull razor algorithm. The Chan-Vese technique was used to segment pictures, allowing them to distinguish between those that had melanoma and those that did not. This research has a 98 percent chance of being correct.

ANN and KNN classifiers were used in a hybrid model proposed by Elgamal and Mahmoud [39] to improve performance (k nearest neighbor). The forward backpropagation neural network is fed by the ANN classifier. This model gathers characteristics from images, categorises them, and decreases the size of each individual attribute. The data set includes forty images (20 benign and 20 malignant melanoma). This hybrid model offers a high prediction accuracy of 97.5%, a sensitivity of 100%, and a specificity of 95% for pictures of melanoma that have been classified as benign or malignant.

Computer-aided diagnostics for tumour diagnosis has been suggested by Ding, Yi et al., [40] The model analyses and categorises texture characteristics that are 3D in the form of natural surface vectors gathered by a stereo optical instrument. For feature extraction, we employ surface rules and a two-dimensional Gaussian model. The ANN front layers are used for classification. The data set includes 34 pictures of benign skin lesions and 12 pictures of malignant melanoma. The model has a sensitivity of 91.7 percent and a specificity of 76.4 percent thanks to the use of CAD technology.

Li, Lin, and colleagues [41] used a novel technique based on single-polarized light spectroscopy and multi-scattered non-polarized light spectroscopy to collect data on the skin's many features. Examining the lesion's skin for tiny patches may be done directly without segmenting the picture. 187 images of skin lesions were gathered for the study. The suggested model's accuracy, sensitivity, and specificity are all at or above 89%.

In a study presented by Zhang, Ni et al. [42], they used a CNN neural network with a whale optimization algorithm in their investigation. They employed two data sets for this method: Dermquest and DermIS, which had over 22,000 dermatoscopy images of skin disorders. When this method was compared to data sets generated in other ways, it came out on top. When compared to the other methods, the proposed strategy outperformed them all. Researchers Chandra.

Theodore Gautama et al. [43] had a different position on the ABCD method's use. A number of factors were found to be incorrect when using this strategy to the detection of melanoma. As a consequence, they employed a grey level co-occurrence matrix to generate a tumor-specific pattern (GLCM) (GLCM). DNN was used to extract and sort the ISIC data set's 870 melanoma photographs and 200 additional images for verification into manageable categories. The findings indicated a diagnostic accuracy of 81.75 percent, a sensitivity of 75.5 percent, and a specificity of 88 percent.

Using a data set of 206 pictures of skin lesions, Wiem Abbes and Dorra Sellami [44] suggested a CAD system to estimate the degree of skin lesions using the DNN method. Skin lesion modelling using bag-of-words is one of the factors used by the algorithm to make judgments (BoW). Fuzzy C-Means is used to calculate the BoW level once the lesion's characteristics are extracted using the ABCD method (FCM). The study's accuracy and sensitivity rates for predicting melanoma illness were 87.5 percent and 90.1 percent, respectively.

Maiti, Ananjan, and Biswajoy Chatterjee [45] improved texturing for 23 dermatological picture attributes in the collection, comprising 170 photos from the MED NODE dataset and 2,000 images from the ISIC dataset. An improved collection

of data was fed into deep neural network models using binary entropy. This method's accuracy at predicting the future was 96.8%.

By merging the neural network with a novel model dubbed the Gray Wolf optimizer (GWO-DNN), Daniel, A. et al. [46] have improved the diagnosis of melanoma. The c-mean approach was used to segment the dermoscopic images and identify the affected regions. Using a gray-level iteration matrix and a DNN classifier using the GWO technique, the ISIC dataset extracts features. In this experiment's description, the suggested model had an accuracy of 87%, a level of sensitivity of 96%, and a level of specificity of 76%. table 2.1 shows all prior research that was considered.

Table 2.1. Review of related literature

Reference	Classifier	Dataset	Description	Result %
Edgar Omar Molina-Molina [26]	KNN	ISIC 2019	Feature extraction, Densenet-201, CAD method.	Accuracy: 97.35 Sensitivity: 66.4 Specificity:97.85
An Gong et al. [27]	CNNs and GANs	ISIC 2018	Classification, feature extraction	Accuracy: 92.4 Sensitivity: 48.3 Specificity: 97.7
Doaa A. Shoieb et al. [28]	CNN, SVM	337 images and DermQuest	CAD method combining the segmentation stage	Accuracy: 94 Sensitivity: 100 Specificity: 88
Mohamed, Abeer et al. [29]	CNN	ISIC 2018	Classification images	Accuracy: 97.78
Soumen Mukherjee et al. [30]	CNN	Dermofit and MEDNODE	CMLD model	Accuracy: 83.07
Sertan Kaymak et al. [31]	AlexNet	ISIC 2018	Classification feature extraction	Accuracy: 84.4 Sensitivity: 84.7 Specificity: 83.8
Lopez, Adria Romero et al. [32]	VGGNet	1279 images of ISIC	transfer learning, Classification, feature extraction	Accuracy: 81.33 Sensitivity:78.66
Albahar, Marwan Ali [33]	CNN	ISIC archive	CNN-Novel Regulaizer , feature extraction	Accuracy: 97.49 Sensitivity: 94.3 Specificity: 93.6
NudratNida et al. [34]	ELM	ISIC-2016 and ISIC-2017	Dermatoscopy, feature extraction	Accuracy: 93
Kanimozhi, T., and A. Murthi [35]	ANN	31 images of different types	Backpropagation, ABCD	Accuracy: 96.9

Dalila, Fekrache, et al. [36]	KNN and ANN	172 of dermatoscopy images	Ant colony-based segmentation	
Sugiarti, Sugiarti et al. [37]	ANN	23 images of different types	MLP method, texture-based trait extraction	Accuracy: 80 and 88.88
SharminMajumder et al. [38]	ANN, Dull razor algorithm	PH 2 dataset	ABCD for feature extraction, Chan-Vese approach,	Accuracy: 98
Elgamal, Mahmoud [39]	ANN and KNN	40 images of different types	Forward backpropagation	Accuracy: 97.5 Sensitivity: 100 Specificity: 95
Ding, Yi, et al. [40]	ANN	46 images of different types	CAD, feature extraction, stereo optical device, two-dimensional Gaussian	Sensitivity: 91.7 Specificity: 76.4
Li, Lin, et al. [41]	ANN, KNN, naïve bayes	187 images of different types	single-polarized light spectroscopy, image processing, c, and classification	Accuracy: 89
Zhang, Ni et al. [42]	CNN	22000 images from Dermquest and DermIS	Whale optimization algorithm	
Chandra, Theodore Gautama et al. [43]	DNN	870 images from ISIC	GLCM matrix	Accuracy: 81.75 Sensitivity: 75.5 Specificity: 88
Wiem Abbes and DorraSellami [44]	DNN	206 images of different types	CAD system, Bow, (Fuzzy C-Means FCM).	Sensitivity: 87.5 Specificity: 90.1
Maiti, Ananjan, and Biswajoy Chatterjee [45]	DNN	170 images from MED NODE and 2,000 images from ISIC	Binary entropy for processing	Accuracy: 96.8
Daniel, A., et al. [46]	GWO-DNN	ISIC archive	c-mean process for segmentation,gray-level iteration matrix for gray-level iteration matrix	Accuracy: 87.98 Sensitivity:96.78 Specificity:76.54

PART 3

CONVOLUTIONAL NEURAL NETWORK

3.1. MACHINE LEARNING

Machine learning is a subfield of artificial intelligence (AI) that allows computers to learn and improve without being explicitly programmed. In other words, it is taking data, analyzing it for similarities, and then making predictions about future events. Machine learning involves creating computer programs that can acquire data and learn independently.

The principle of machine learning is to work with observable data so that you can look for patterns in evidence and make better decisions based on the indicators provided. As a result, it entails discovering patterns in the data (data mining) and using those features to identify or forecast a problem-related occurrence [47].

The primary goal is for computers to learn independently, without the need for human participation, and to change their behavior appropriately. Computer scientists may increase the accuracy of a machine learning model's predictions by continuously feeding it more data. Various types of machine learning have evolved from this basic principle. One of the main approaches used to classify this type of infrastructure according to the learning approach is used in every aspect of machine learning research [48].

3.1.1. Supervised Learning

Supervised machine learning uses predefined (labeled) output and input features [47]. This method is used to deal with data that has been categorized, and this

strategy is less complicated to perform in learning methods. The key benefit of this echnology is the ability to collect or develop data outputs from prior information. The disadvantage of this strategy is that when the training set lacks the samples that should be in the class, the classification algorithm may be overdone.

3.1.2. Unsupervised Learning

Unsupervised machine learning is a kind of machine learning in which the system is not monitored. You should instead let the model to determine its own informational requirements. It mostly focuses on unlabeled data. Unsupervised learning provides for more complicated data processing than supervised learning [48].

Unsupervised learning algorithms use Integrating and feature minimization to employ previously learned features to identify data classes while adding new data [48,49].

3.1.3. Semi-Supervised Learning

Semi-supervised learning may be used on both labelled and unlabeled data. As a result, semi-supervised machine learning combines the best features of both supervised and unsupervised learning. It may be especially advantageous in domains like statistics and machine learning if there is existing unlabeled data and classifying it is a time-consuming job. The most convincing machine learning algorithms may be taught on "processed" data sets incorporating score information. This method teaches people how to commit to ambiguous data [50–52].

3.1.4. Reinforcement Learning

Reinforcement learning (RL) is a machine learning paradigm that leverages the snip method to train an algorithm. After every action, the system (agent) examines the current

Condition (state), acts accordingly, and takes input (reward) from the surroundings. Positive responses are a reward (in the sense that we understand it), while negative responses result from making an error [50,53].

3.2. DEEP LEARNING

The several-layer deep learning model is a represented training algorithm that turns raw data into the representations needed for pattern classification without considerable human interference. A deep learning platform's layers are structured in a logical order and contain many preset nonlinear processes [54,55]. One layer's result is transmitted to the next, resulting in more sophisticated and abstract models. The deep learning approach may learn specific procedures in this manner.

Because they can run on specialised computer hardware, deep learning algorithms can handle vast volumes of data and be updated with fresh data. Product categorization, translation software, and natural language processing are data-intensive applications [55]. Due to the vast volume of medical data, deep learning significantly impacts the medical field. Deep learning's effectiveness in solving society's most difficult challenges can be attributed to various reasons, including [56]–[58] :

1) With the application of information technology, large amounts of training data are available.

2) High-performance computing resources are abundant.

3) Deep learning systems are available, including GoogLeNet, ResNet, and DenseNet.

Deep learning techniques are usually trained and supervised, which means that the training datasets include both pieces of data (for instance, images of skin diseases) and data labeling (for instance, "benign" or "malignant") at the same time. However, since

identifying vast amounts of data is expensive and complicated, data tags are restricted to health records.

3.2.1. Convolutional Neural Network

network. A network comprises a collection of coupled neurons grouped into different tiers. The neuron evaluates a function on the input of the previous layer and transfers the data (the activity of the neuron) to the output of the next layer [61] Although all neurons in each layer perform the same function, known as neurons, they may have varying combinations of inputs and outputs and varied weights assigned to their inputs [62] .The input layer of the network receives a super vector input. This data is disseminated over a network of interconnected tiers (hidden layers). Figure (3.1) depicts the three fundamental layers of a typical CNN: the Convolutional Layer, the Pooling Layer, and the Fully-Connected Layer.

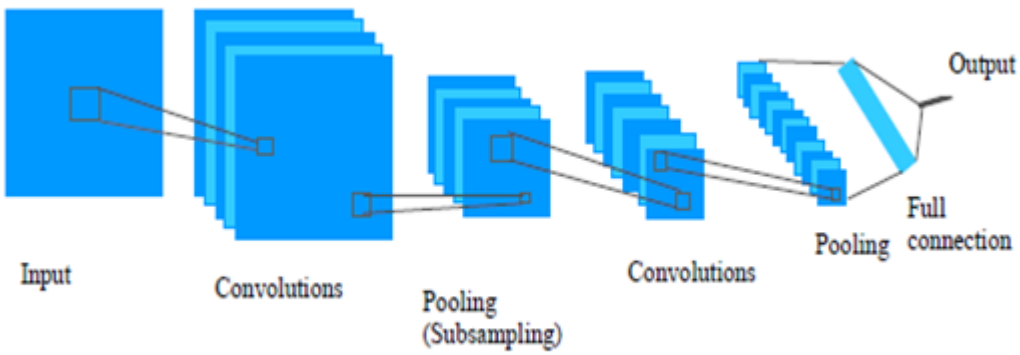

Figure 3.1. A typical illustration of the convolutional neural network [63].

3.2.1.1. Convolutional Layer

A convolutional neural network's fundamental construction element is the convolutional layer. Kernels are trainable filters that make up the parameters for convolutional layers [64]. This layer is where the majority of the computations are done. Each filter is made up of a small section of the image. The filter comprises a set

of values on a neural network layer of a certain size. The filter's parameters are increased by the input pixels. Each convolutional layer contains a series of filters, which form a 2D output matrix when moved across the receptive field [65], as shown in figure (3.2). The number of pixels employed in learning to seek anything different in the input correlates to the depth. If the actual image's input is used as the initial convolutional layer's input, distinct neurons throughout the hidden layers will be engaged. When traversing the filter through the input matrix, stages are established when there are distinct edges, colors directed, and so on.

Activation layers aren't actually "layers" (since no guidelines are established inside an activation layer), and they're often left out of core network schematics because it's expected that activation happens right after a convolution. Various activation functions can be utilized in the activation layer [66]

- **Sigmoid Function**

The sigmoid function is a non-linear activation function in neural networks often utilised in feed-forward networks. A variation function is one that uses real input data to run functions with positive derivatives. Sigmoid functions are used to forecast likely outcomes in deep learning models' output layer. The sigmoid function is written as follows [66-67]:

$$\sigma(x) = 1/(1+exp(-x)) \tag{3.1}$$

Generally, the derivatives of the sigmoid function are applied to learning algorithms. Some of the sigmoid function's major obstacles include languid assemblage and squeaky gradients during back-diffusion from deeper hidden layers to the input. The graph in (3.3) depicts the various formats of the activation function. [67].

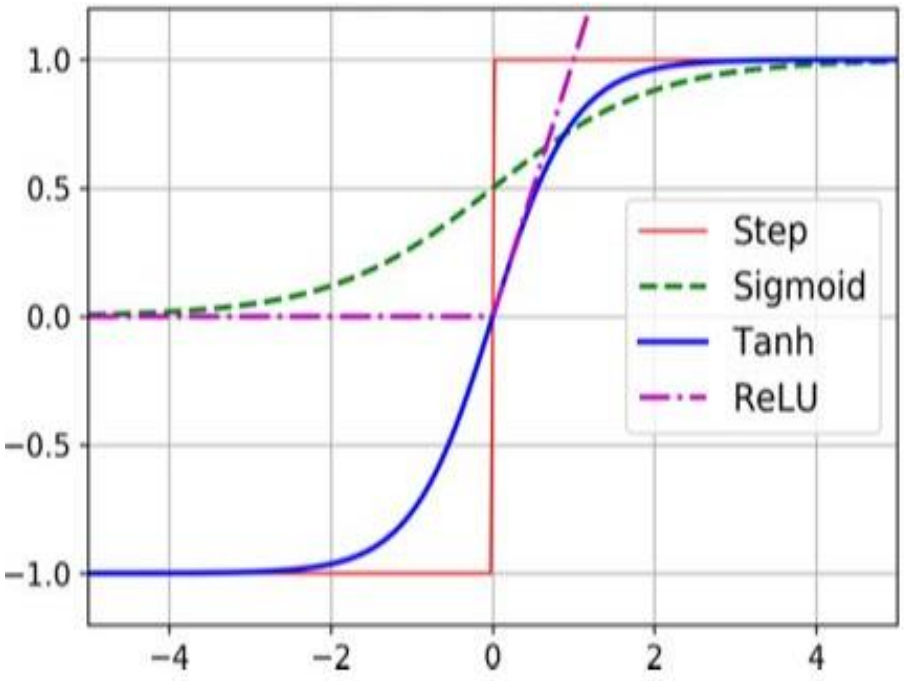

Figure 3.2. Display activation formats

- **Tanh Function**

The nonlinear activation function, often known as the tanh function, is another kind of AF. With a range of -1 to 1, this function is more rounded and zero-centered. As a consequence, the output of the tanh function is expressed as [66]:

$$f(x) = tanh(x) = \frac{2}{1 + e^{-2X}} - 1 \tag{3.2}$$

The tanh function is used more often than the sigmoid function because it provides higher performance for neural networks with several layers. The primary advantage of the tanh function is that it produces a zero-centered output, which aids in back propagation

- **Rectified Linear Unit**

Rectified linear unit (ReLU), a quick activation function that strives to give cutting-edge performance with outstanding outputs, is one of the most prominent activation functions (AF) in deep learning. ReLU is superior to other activation functions in terms of performance and flexibility in deep learning. The function is almost linear and preserves the characteristics of linear models, which makes gradient-descent approaches easier to optimise. [66], [68].

The ReLU function is applied to each input element as a threshold operation, resulting in all values less than zero being set to 0. As a result, the ReLU is represented as:

$$f(x) = max(0, x) \tag{3.3}$$

This function addresses the degradation problem by resetting to zero the amounts of inputs that are less than zero. The primary benefit of using the ReLU function in the calculation is that it expedites computation by eliminating the need to compute exponents and divisions, resulting in a faster total computation. The ReLU function generates sparsity in the hidden units by compressing the values between 0 and their maximum. [66–68].

- **Softmax Function**

As an activation function for generating a posterior distribution from a vector of real numbers, neural networks use a softmax function. This function returns a number between 0 and 1, with one possible outcome. Syntax for the softmax function is as follows:[66],

$$f(xi) = \frac{exp(xi)}{\sum exp\ (xj)} \tag{3.4}$$

This function is extensively used in multi-class models to provide likely outcomes for each class, with the target class having the highest success probability. It is used by almost every output layer of the deep learning architecture, including the multidimensional classification levels.

3.2.1.2. Pooling Layer

The pooling layer, also known as the down-sampling layer, reduces the output feature size of the convolution layer to reduce the number of variables and calculations required by the network. Overfitting is also controlled using the pooling layer [69,70]. The pooling layer is usually chosen between the two wraparound layers, convolution and fully connected layers. Two of the most common approaches are maximum pooling and intermediary pooling [71].

The maximum pooling for a certain window sets the largest value in that frame, while the mean pooling gets the average of the data in that frame (fig. 3.6). Window size and phase value are two critical hyper-parameters for the assembly operation. Network data representations are gradually reduced, which helps in configuration management. This class does not learn any parameters; instead, it creates new spatial inputs the size of the

Next convolution layer without adjusting depth or feature assignments and keeps edges in place.

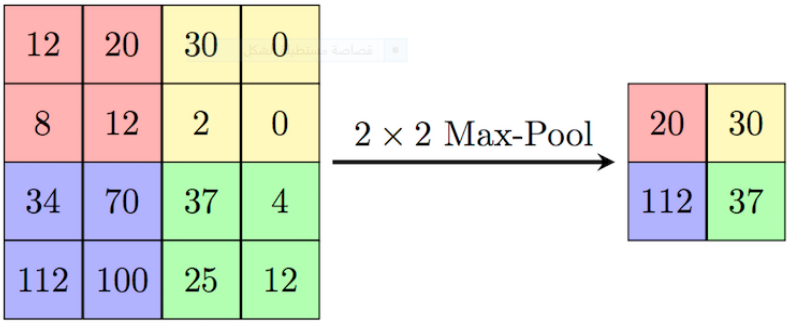

rFigure 3.3. Procedure of pooling laye

3.2.1.3. Fully Connvolutonal Layer (FC)

These are the completely linked layers at the end of a convolutional neural network (FC). Each neuron takes information from the previous layer's elements. The responsive domain includes the entire previous layer [72]. The receptive area in the convolutional layer is smaller than the prior layer (figure 3.7). The widths among these layers are commonly retrieved as 4D or 3D features that are compressed to identify the photos before passing through the softmax unit. FCN is composed only of convolutional layers. Consequently, the last completely connected layers are similarly convolutional. [73]. Sensors learn hierarchical structures that integrate multi-band fields to accommodate low, medium, and high-level information within contour and object borders.

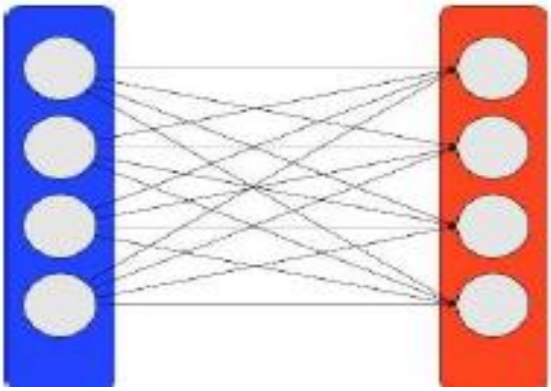

Figure 3.4. Display fully connected layers.

3.2.1.4. Dropout layer

Dropout layers have the purpose of reducing overfitting and improving prediction error. The model may classify training samples correctly but does not operate well on data that has not been seen before. By adjusting the dropout layer to zero, the objective is to neglect a random collection of activations in that layer. A dropout layer is only used in the training phase. It prevents the system from overfitting the data for training [74–76]

3.2.1.5. Batch Normalization

The goal is it to improve neural network speed, execution, and stability by normalizing the input layer and adjusting the calibration [76].

3.3. DENSE LAYER

Numerous new deep learning models have been developed, but they all come under the convolutional neural network umbrella. Among these models are VGG, ResNet, DenseNet, GoogleNet, and AlexNet.

We'll talk here about the DenseNet features we used in our research. Each layer in DenseNet receives extra input from the preceding layer and sends its feature mappings to higher tiers. It is used to create a sequence. All the preceding layers provide "shared wisdom" for each layer. The network can be smaller and more compact since each layer gets image features from all preceding layers, reducing the number of connections. The growth rate k represents the rise in the number of layers per layer. As a result of its enhanced computational and storage efficiencies, [77–79]. Figure (3.8) represents the block design for the dense layer.

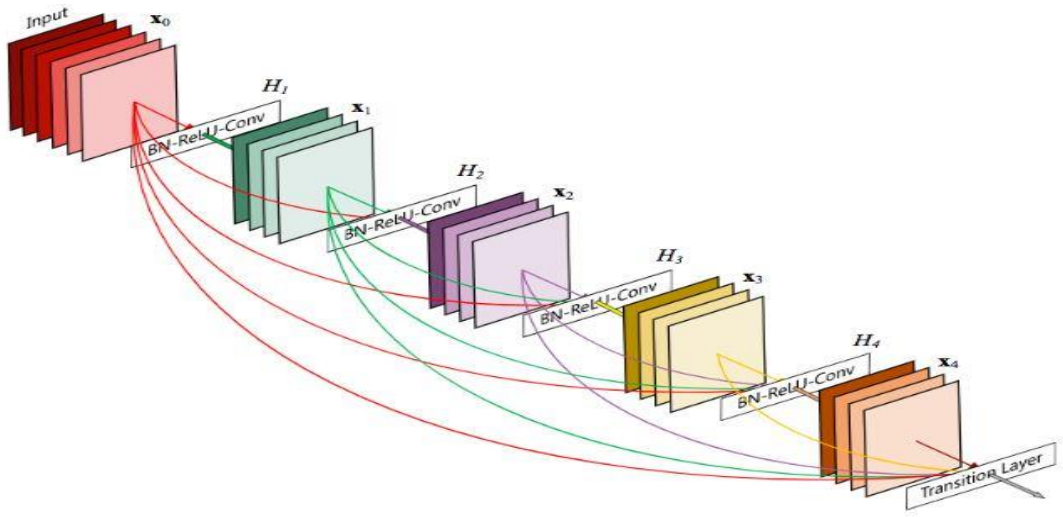

Figure 3.5. Five-layer dense block using all previous feature maps as input. [80].

Huang proposed DenseNet, a densely connected design with properties that distinguish it from its nearest competitor, ResNet [74]. DenseNet is similar to ResNet in terms of ideas, although there are some variances. It has refined its technique to handle the color spectrum issue using cross-layer interaction. A feed-forward strategy was used to connect each layer to all other layers in the network. The next layers were inserted using the image features from the preceding layers [81]. It has the benefit of being able to differentiate between new and retained information because it concatenates rather than adds characteristics from prior layers.

With all of the previously mentioned benefits, this model has one drawback: it is borderline pricey, as well as the expanding number of feature maps [78]. The loss function facilitates the flow of information throughout the network by allowing all levels to take gradients directly. This also includes a structural impact that lowers task over-allocation when short training sets are used [74,77,78].

3.4. PERFORMANCE METRICS

Many parameters are used to accomplish an accurate and unambiguous assessment of deep learning models that are trained using datasets. Several important criteria were selected to assess performance in this study since these values were represented in our research.

3.4.1. Accuracy

Calculates the true proportion of cases diagnosed by predicting the number of real illnesses [82].

$$accuracy = \frac{\text{true detected cases}}{\text{all cases}}$$

$$ACC = \frac{\text{TP+TN}}{\text{TP+FP+FN+TN}} \tag{3.5}$$

3.4.2. Sensitivity

It estimates the exact number of true positive instances and identifies the true injury cases [83].

$$sensitivity = \frac{\text{true detected melanoma cases}}{\text{all melanoma cases}}$$

$$SE = \frac{\text{TP}}{\text{TP+FN}} \tag{3.6}$$

3.4.3. Specificity

It estimates the precise proportion of true negative instances and the number of real injury cases [84].

$$specificity = \frac{\text{true detected non melanoma cases}}{\text{all non melanoma cases}}$$

$$SP = \frac{\text{TN}}{\text{TN+FP}} \tag{3.7}$$

3.4.4. Positive Predictive Value (PPV)

It is a method for identifying and assessing positive cases, whether true or false positives [85].

$$Positivr\ predictive\ value = \frac{\text{true detected non melanoma cases}}{\text{deceted non melanoma cases}}$$

$$PPV = \frac{\text{TN}}{\text{TN+FN}} \tag{3.8}$$

3.4.5. NegativePredictive Value (NPV)

The percentage of anticipated negatives turns out to be true negatives. It expresses the likelihood that a predicted negative is true [86].

$$NPV = \frac{\mathrm{TN}}{\mathrm{TN} + \mathrm{FN}} \tag{3.9}$$

3.4.6. Precision (PRE)

It is the proportion of relevant examples found among the effects, whereas recall is the proportion of relevant items found [86].

$$Pre = \frac{\mathrm{TP}}{\mathrm{TP+FP}} \tag{3.10}$$

3.4.7. F1-Score

Considering a model and some fresh input, refers to the process of creating new outcomes.

$$F1 = 2\,x\,\frac{Pre\,x\,SE}{Pre+SE} + \frac{2\,x\,TP}{2\,x\,TP+FP+FN} \tag{3.11}$$

3.4.8. Reciever Operating Curve (ROC)

The AUC calculates the effectiveness across all potential classification levels by measuring the complete two-dimensional area beneath the ROC curve. One approach to analyzing AUC is the likelihood that the model rates a randomized positive example higher than a randomized negative one [87].

PART 4

METHODOLOGY

In this section, we will talk about how to collect and prepare data while mentioning the platforms used, including the available Python libraries used in the research. Next, we will discuss the method of distributing and dividing the data. Finally, we will discuss how we designed the proposed system and how we will implement it.

4.1. DATA COLLECTION

Data collection is crucial since recent deep learning algorithms have less of a requirement for feature engineering and a need for large amounts of data. We investigate data validation and cleaning strategies to improve data quality. Even though the data cannot be completely cleansed, utilizing training techniques, we can still deal with poor data during model training

Eight datasets were used, which to our knowledge, is the most data used in providing images of skin lesions in medical and research centers. Most of these data sets are freely available on the internet. They are obtained from Github, an open-source website offering free Python simulation datasets; some require certain subscriptions. Table (4.1) shows the datasets used with the number of image data for each set.

Table 4.1. Displays number of images for each dataset

Dataset	No. of origin images
HAM10000	10015
ISIC 2019	8520
DermIS-DermQuest	6600
ISIC 2017	6030
ISIC 2016	6400
MED-NODE	4332
PH² dataset	200
DermNet	571

The eight data sets used in this research contained seven categories of skin lesions, and some of these data contained 21 sub-categories. Each data set contains several images obtained by the dermatoscopy method. The common factor in dividing this data is that it contains two main categories: benign and melanoma.

To facilitate the classification process, each category of skin lesions is encoded with a special symbol, as shown here: ‘nv’= ‘melanoma nevi’ , ‘mel’ = ‘melanoma’ , ‘bkl’ = ‘benign keratosis-like lesions’ , ‘bcc’ = ‘maligna melanoma’ , ‘vac’= ‘pyogenic granulomas and hemorrhage , ‘akiec’ = ‘Actinic Keratoses and intraepithelial carcinoma’ , ‘df’ =‘dermatofibroma’.

4.2. DATA PREPARATION

4.2.1. Platform Used

This project used a Lenovo laptop with an Intel(R) Core (TM) i5-7200CPU@ 2.5 GHz 2.7 GHz, 64 bits 6th generation, 8GB RAM, Windows 10 OS, GPU CUDA support for NVIDIA GeForce GTX 1060, and Windows 10 OS.

4.2.2. Initializing Libraries

There are various packages were used to implement the project:

- **Keras**

It is a Google-developed high-level deep learning API for the creation of neural networks. Python is used to simplify the process of constructing neural networks. Using this method, many neural networks may be calculated on the backend. [88,89]

- **Tensorflow**

TensorFlow is a computational intelligence library created as an open-source project. Classical machine learning is also supported. TensorFlow was created to perform huge arithmetic operations. The TensorFlow library can be imported into our Python environment and used for extensive educational development [88–90].

- **Scikit learning**

It is the most accessible and effective machine learning software for Python. It supports machine learning and data mining techniques like as classification, regression, grouping, and dimension reduction through its Python consistency API. [90].

- **Numpy**

It's a Python research library, and working with array structures and linear algebra processes is an important feature of deep learning. NumPy is frequently used with Python scientific tools such as SciPy and Matplotlib. This combo is frequently used as a replacement for MatLab, a well-known scientific computing platform [91,92].

- **Matplotlib**

It's a Python research library, and working with array structures and linear algebra processes is an important feature of deep learning. NumPy is frequently used with Python scientific tools such as SciPy and Matplotlib. This combo is frequently used as a replacement for MatLab, a well-known scientific computing platform [91,93].

4.2.3. Data Splitting

It is optimal to divide the data set into two training and testing sets in a ratio of 1/3, with the training set being the largest portion and the test set the smallest. Prior to using a test set, it is important to train the model.

Multiple strategies exist for preventing overfitting, including splitting the data set into training and test sets. The accuracy of the model's performance evaluation depends on the similarity between the patterns in the training and test sets and the real data.

Set validation is essential when we need to choose between various models and evaluate which one performs better, regardless of the model's performance. In figure (4.1), there are some photos from datasets used in the splitting process.

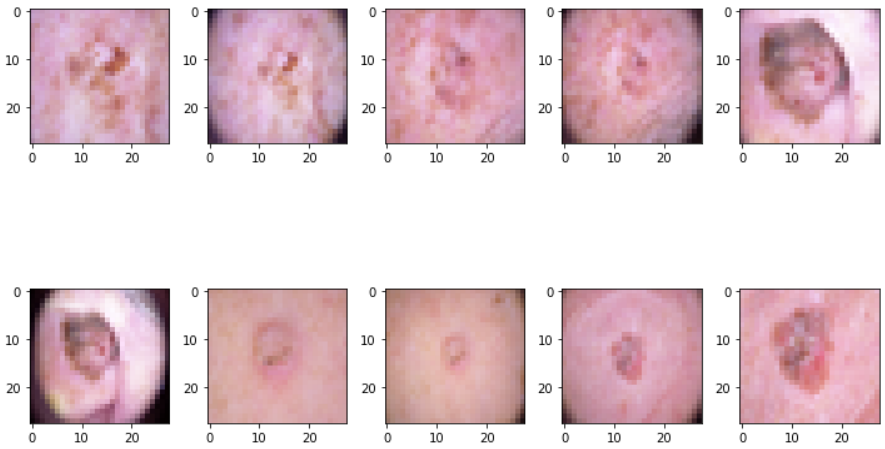

Figure 4.1. For example, standardization and splitting data

After resizing the images and adjusting the size to be f.set_size_inches(10, 10) and reshaping them to be reshaped (28,28,3), random skin lesions images appear in the image (4.2)

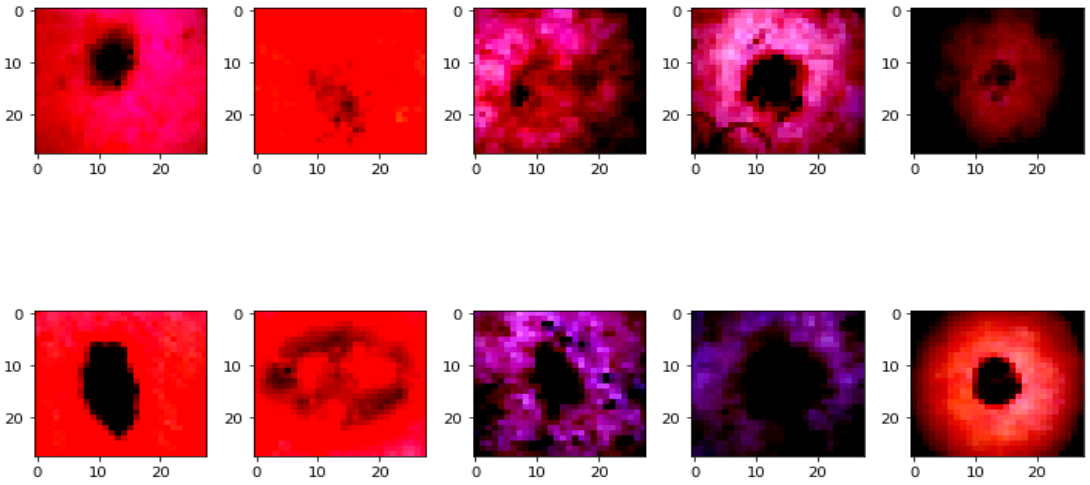

Figure 4.2. For example, standardization and splitting data, after reshaping and resizing

4.2.4. Data Augmentation

The proposed technique uses TensorFlow data augmentation functions like random flip (up-down and left-right). Using augmentation is the only way to teach an image to be accurate in real-world situations.

Neural networks must undergo extensive training to handle massive amounts of data [34] successfully. The arrangement of images used in learning may be inadequate or imbalanced. Reproduction is carried out in the dataset to enhance the rate of incomplete evidence used in education. Photo augmentation is a breeze with Keras' built-in libraries. Additional data for the training dataset is generated via the data replication method. It's done in various ways, including rotating, scaling, translating to the main image, and mixing these techniques [37,38,63].

In this study, we use a random rotation angle variety within the spectrum of [0, particular angle]. Each of the trained dermatoscopy images in each of the eight datasets was rotated four times at 0°, 90°, 180°, and 270° angles. Figure (4.3) illustrates the

effect of data augmentation. By improving the data, we boosted the pictures of the basic training set in all datasets utilized here.

Figure 4.3. Example of melanoma Images after data augmentation

4.2.5. Data Allocation

The data about a set of the gathered information is organized and displayed using feature representation. Deep learning data with a statistical distribution is advantageous for model construction. Since Python dynamically resizes images to approximate small pixels, the present project chose elevated images of 224 x 224 pixels rather than small pixels and converted them to 28 x 28 pixels through resizing. Initially, the data set was distributed into two groups: test and training. Seven categories of skin lesions were distributed to each group, Figure (4.4) shows the process of dividing the seven categories of melanoma into the training category and the verification category.

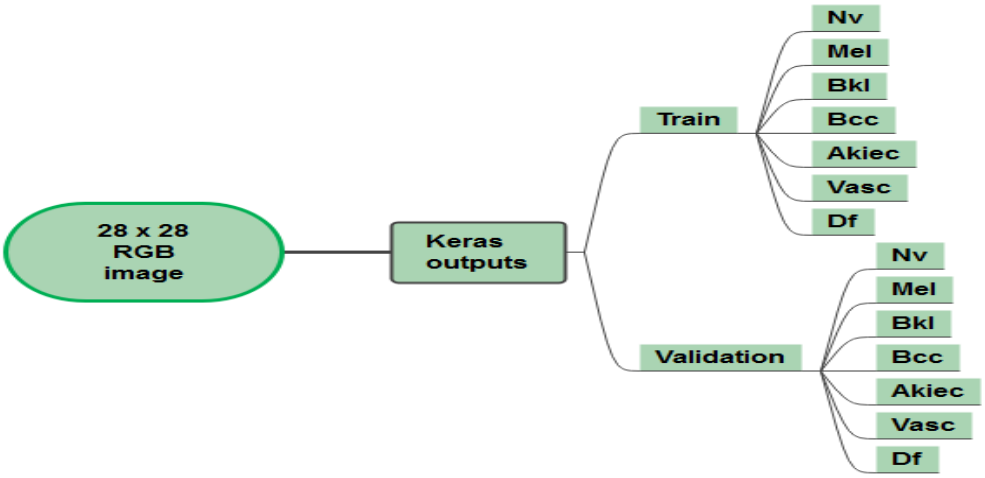

Figure 4.4. Shows the distribution of skin cancer classes

4.2.5.1. Classes-Based Distribution

The seven skin lesions were distributed after changing the size of each figure to become "disease" size=20, and the frequency changed to become "frequency" size=20). The graph has been configured in Python to be (0.5, 1.0, 'Frequency Distribution of Classes'), as shown in figure (4.5).

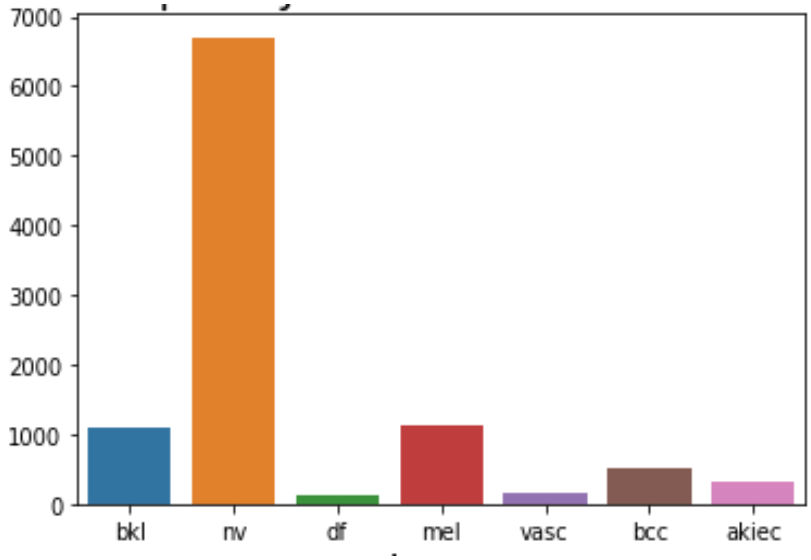

Figure 4.5. Frequency distribution of classes

4.2.5.2. Gender-Based Distribution

We note in the previous scheme (4.5) that the data distribution was in the form of an unbalanced, but when distributing the data based on gender, it became almost balanced, as shown in figure (4.6). So, the data was divided by 54% for men, 45.5% for women, and 0.6% for unknown.

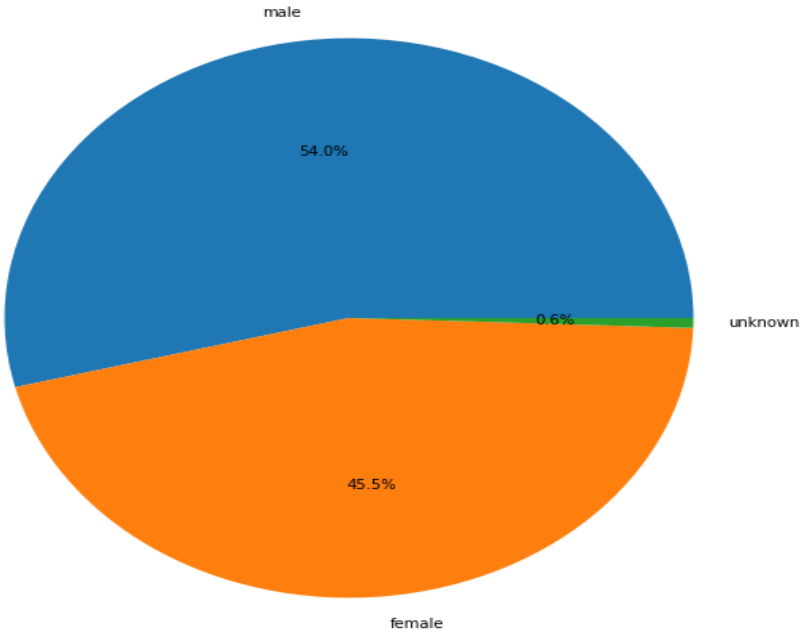

Figure 4.6. Patient gender distribution

The skin lesions were also distributed to all parts of the body, numbered fifteen (15). Images are resized for gender, disease category, image size, and rotation adjusted so that fig size = (12, 12), "Gender", size = 16, "Disease", size = 12, "Frequency/Count", size = 12 and rotation = 90. Figure (4.7) shows the distribution of diseases according to sex in all body parts.

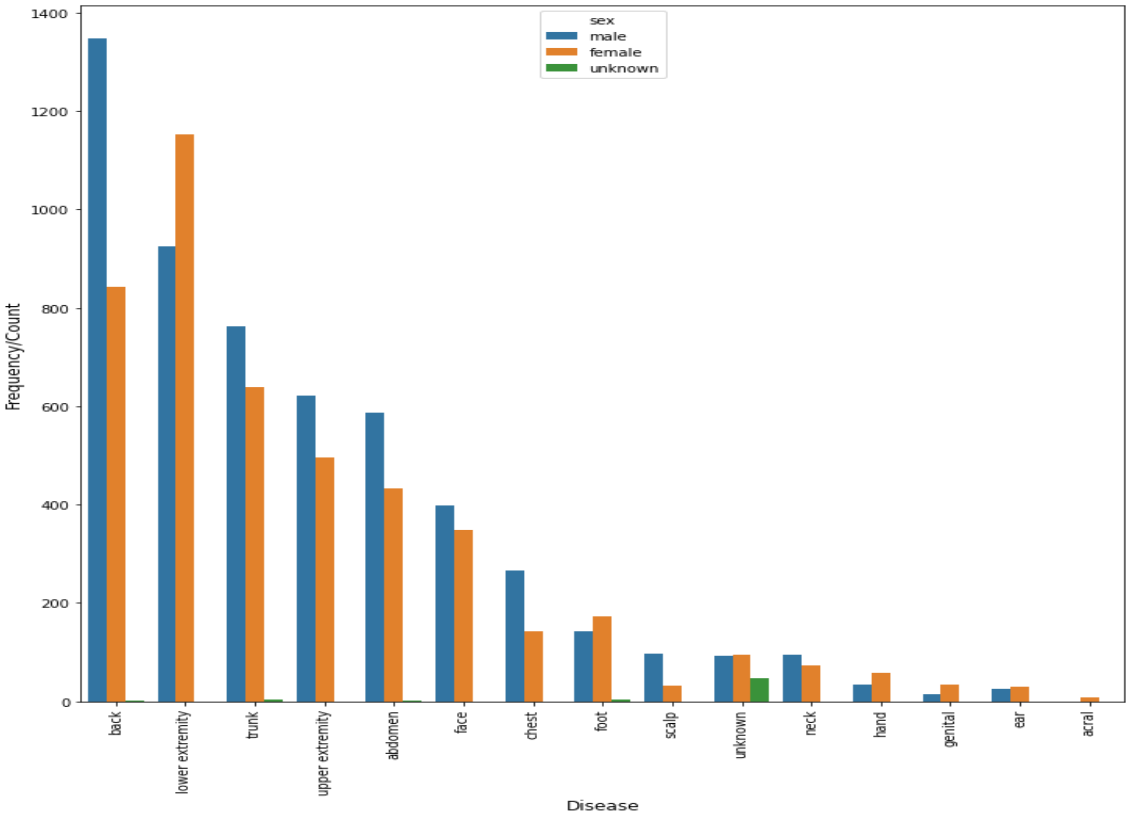

Figure 4.7. Example for standardization and splitting data

4.2.5.3. Age-Based Distribution

The pictures were distributed based on the patient's age, and the pictures' size was adjusted to fig size = (10,10). Figure (4.8) shows the distribution of the pictures, and it becomes clear that the largest percentage of injuries ranged between the ages of 45 and 50 years.

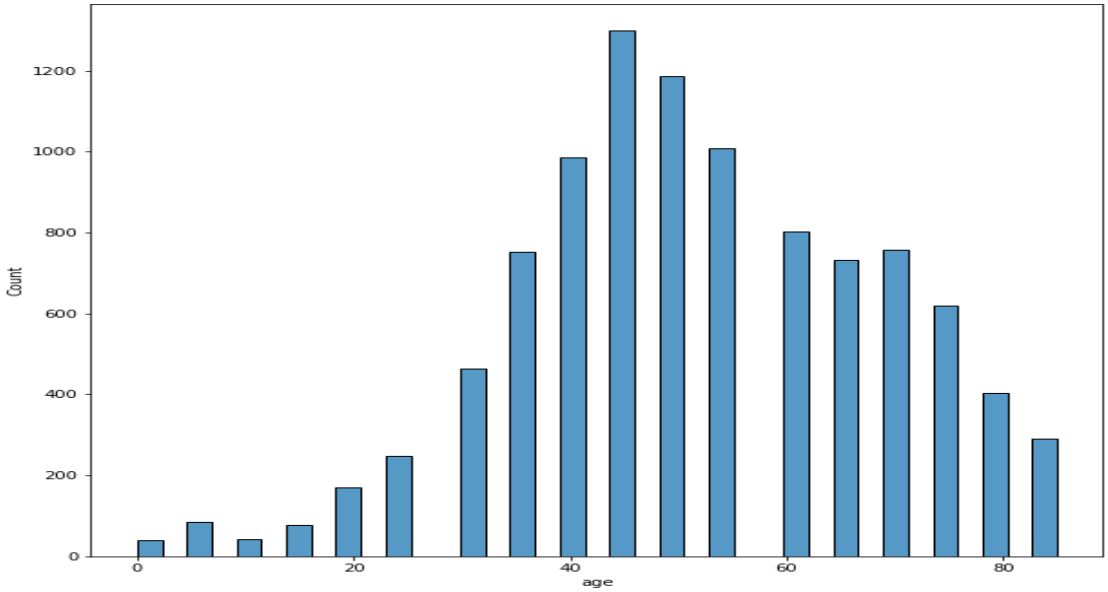

Figure 4.8. Histogram of the patient's age

4.3. PREPROCESSING

Preprocessing is a technique for removing noise and blemishes from images and visually superfluous data. Additional preprocessing procedures could include a spatial reduction (lowering the number of bits per pixel or the image size) and locating regions of the image for more processing. Light and noise impacts are common in skin surface images when taken with expert image sensors, so they must be removed [59,91]. These effects include non-uniform lighting and light-reflective surfaces on the skin's surface.

First, lighting is used to minimize the impact of these variables on CNN classification. On the input images, the adjustment step is carried out. At this stage, it detects lighting impacts as sharp changes in the absorption and valuation streams for the color space. As a result, the lighting impacts are overlooked with a particular set of contours. This is done without trying to destroy the initial image's actual factual edges

The image includes both clear skin and a lesion. This has the potential to misinform CNN training. Areas of healthy people are an ineffective set of criteria for sensing skin cancer. In the meantime, creating and improving can result in data loss, such as the

color intensity between the abscess and the patient's normal skin [28]. Such data can serve as a discrimination guide. The cipher mask is used for this intent.

4.3.1. Data Cleaning

The missing data and duplicated data are examined at this stage. Missing data can be dealt with in a variety of ways, including substituting the quantity with the attribute's average [95]. Discrepancies in the data were discovered and omitted by checking the criteria recognized by this study.

4.3.2. Data Normalization

Normalization is a data preprocessing technique that is frequently used in deep learning. The method aims to translate the values of numerical columns in a dataset to a similar scale without altering the value ranges.

In this study, we solved the model learning trouble by ensuring that the various characteristics had comparable value ranges so that gradient descents could converge faster.

4.4. OVERSAMPLING

Random oversampling includes adding additional duplicates of some of the class labels to the training data. The number of data points, copies of previous samples, is increased randomly for the imbalanced class. This should provide us with a reasonable amount of data to experiment with. Oversampling could result in overfitting of the training data, as shown in figure (4.9)

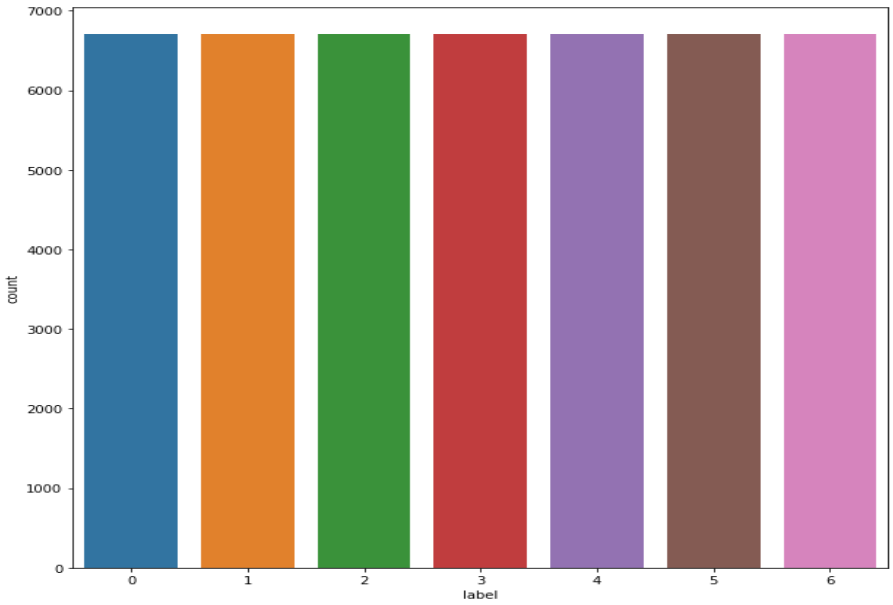

Figure 4.9. Random Oversampling

4.5. OBSTACLES

The difficulty of finding the correct datasets for training models is known as "data acquisition." As the number of data sets available varies, it becomes increasingly difficult to find the right data sets. All supervised learning approaches involve data labelling. Because manual labelling can be costly, numerous scalable solutions based on semi-supervised learning have been suggested.

We encountered some difficulties in developing the data collection method, the most significant of which was the categorization issue. If too few examples have one or more subcategories between the classifications, we may have difficulties with imbalanced classifications in the data. Also, because the model cannot read the basic data in real time correctly, the data disorder causes the incidence of not good [96].

Once the data has been obtained, we must determine if the quantity is enough for the use case. We have considered that the information obtained is time series, and we consider that the data collected is recent; that is, the period of its creation does not exceed 8 years. Another challenge we had while working on our project was

determining the best classification model and training the model using the data we collected.

4.6. SYSTEM IMPLEMENTATION

4.6.1. Proposed Model

This section will detail the steps for creating the proposed architecture, including mentioning the libraries on which the architecture is based. We will support building architecture with diagrams, tables, and illustrations explaining the functions used in the proposed model.

The Dense-convolutional neural network (CNN) model was developed to identify melanoma as malignant or benign. The architecture consists of four basic layers: the Conv2D layer, the MaxPool2D layer, the flattening layer, and the dense layer. Function layers consist of the Relu layer and the softmax layer. After processing, the images consist of (preprocessing, segmentation, feature extraction, and classification), as shown in table (4.2). Building and organizing the basic layers was the first phase, followed by testing the series of training steps and activation functions and ultimately introducing the optimizer to the model.

Adam's optimizer was used to examine how data augmentation influences prediction accuracy in this experiment. When we compared the algorithm's effectiveness to earlier work on the same model, we discovered that Adam's optimizer is a better data optimizer than others. The activation functions will return a maximum value of (0, x). It will return x if the relationship between x and 0 is higher than 0. This function returns 0 if it is not called.

A hyperparameter is the magnitude of the zero padding. When filters are applied to an input matrix, the resulting volume's spatial size shrinks. The size of the output produced will shrink when more convolutional layers are applied. However, to obtain low-level characteristics from the margins of images, it is sometimes preferable to

keep as much data from the source input matrix as possible. As a result, the output volume emphasis is frequently kept the same as the input volume. Zero padding is a feature that allows you to customize the output volume's spatial size. It pads the input space with zeros around the boundary [33,34]. The proposed model for skin cancer diagnosis is shown in figure (4.10).

Table 4.2. Dense sequential model

Layer (type)	Output Shape	Param #
conv2d (Conv2D)	(None, 28, 28, 16)	448
conv2d_1 (Conv2D)	(None, 26, 26, 32)	4640
max_pooling2d (MaxPooling2D)	(None, 13, 13, 32)	0
conv2d_2 (Conv2D)	(None, 13, 13, 32)	9248
conv2d_3 (Conv2D)	(None, 11, 11, 64)	18496
max_pooling2d_1 (MaxPooling2D)	(None, 6, 6, 64)	0
flatten (Flatten)	(None, 2304)	0
dense (Dense)	(None, 64)	147520
dense_1 (Dense)	(None, 32)	2080
dense_2 (Dense)	(None, 7)	231

Total params: 182,663
Trainable params: 182,663

Non-trainable params: 0

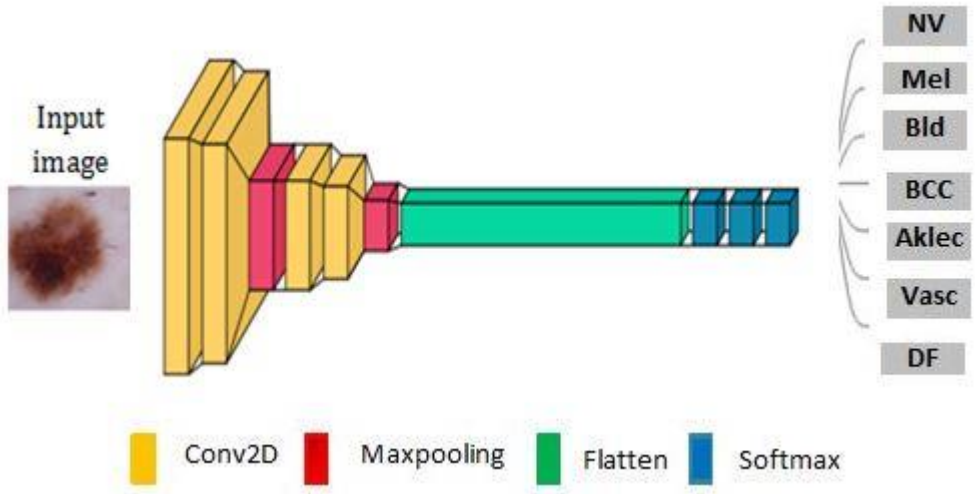

Figure 4.10. The model that was proposed and designed by us

4.6.2. Proposed Dense Layer Architecture

The images are inserted into the Conv2D layer of kernel size (28, 28) pixels and stride (3) pixels so that it becomes an input shape of kernel size (28, 28, 3) pixels, and the output is (28, 28, 16) pixels. Then the same size of the first input is fed to a second Conv2D layer. After that comes the max-pooling layer with a kernel size of (26,26) pixels and a stride of (32) pixels, so it becomes an input shape of kernel size (26,26,32) pixels, and the output is (13,13,32) pixels. The next layer is the Conv2D layer with kernel size (13, 13) pixel and stride (32) pixel, so it becomes an input shape of kernel size (13, 13, 32) pixel, and the output is (13, 13, 32) pixel. After that, added another Conv2D layer with kernel size (13, 13) pixel and stride (32) pixel, so it becomes an input shape of kernel size (13, 13, 32) pixel, and the output is (11, 11, 64) pixel.

The next layer is max-pooling with kernel size (11, 11) pixel and stride (64) pixel, so it becomes an input shape of kernel size (11, 11, 64) pixel, and the output is (6, 6, 64) pixel

.

Then comes a flattening layer with an input of kernel dimension of (6 x 6) pixel and a stride of (64) pixel, so it becomes an input shape of kernel dimension (6 x 6, 64) pixel, and the output is (6 x 6, 64) pixel. The comes is a Dense layer with a kernel size

of (6 x 6) pixel and a stride of (64) pixel, so it becomes an input shape of kernel size (6 x 6, 64) pixel and the output of matrix shape is (None, 64) pixel.

The next layer is a Dense layer with a size of (None, 64) pixels of the output matrix shape, and the output is (None, 64) pixels. Then the next layer is a Dense layer with a size of (None, 32) pixels of the output matrix shape, and the output is (None, 7) pixels. Finally comes the activation layer, consisting of two layers: the Relu layer and the softmax layer. Figure (4.11) shows in detail the stages of architectural completion.

The number of epochs is 50, which acts like training the data. The flattening layer acts to convert the next multilayers to one layer to introduce them into the final layer to facilitate the process of getting output. Figures (4.11) and (4.12) are design blocks that help us understand the architecture quickly.

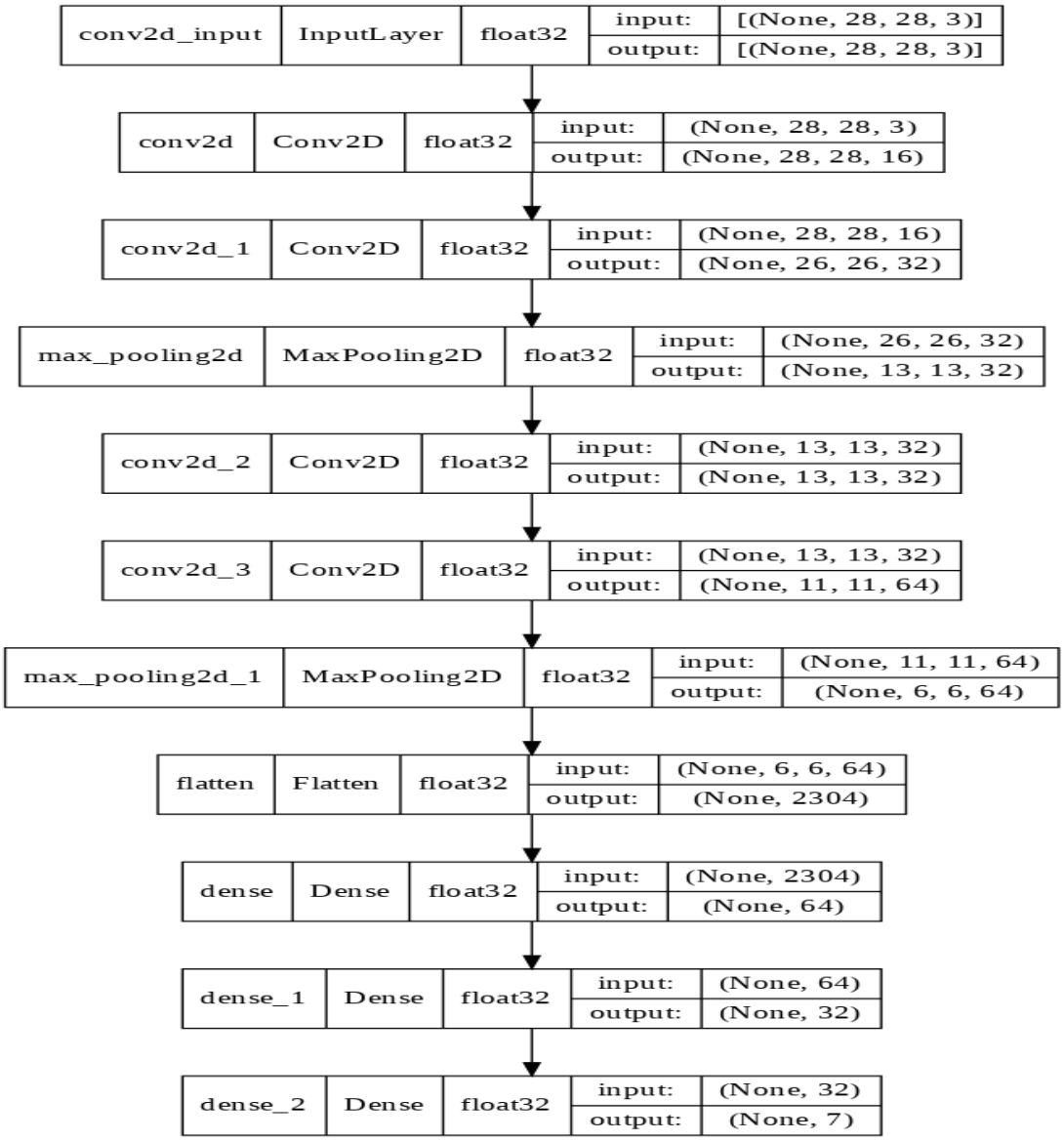

Figure 4.11. Sketch of the melanoma detection model

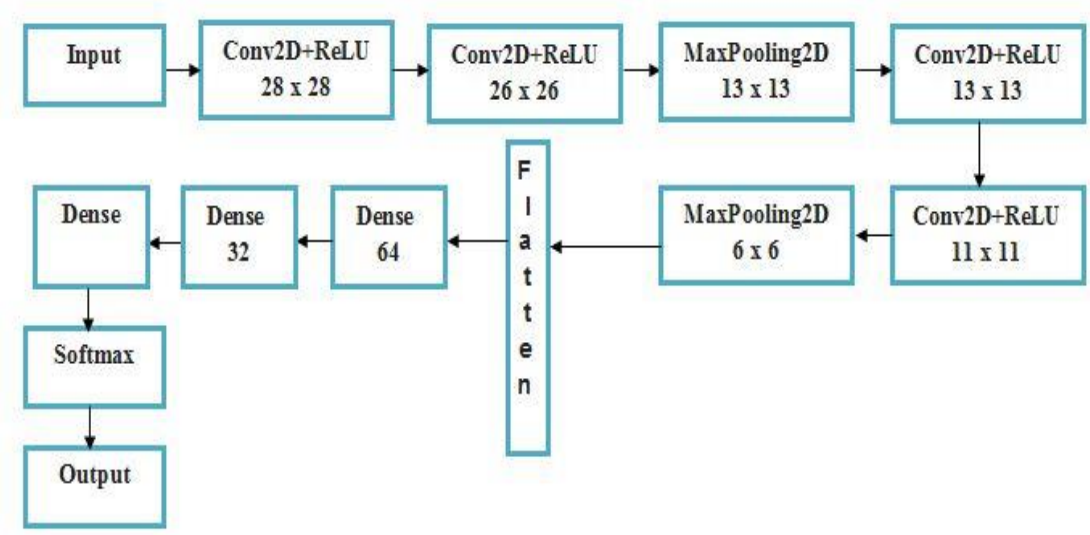

Figure 4.12. Flowchart of block of proposed system

4.6.3. Model Training

Training and evaluation data were isolated from the remaining data. The model is trained using the training data, while it is tested with new data. The issue of overfitting arises when the model is trained on the training data correctly, with a low false-positive rate, but performs poorly on the test data, with a high failure rate. Regulation is one of the approaches used to resolve the challenges of overfitting and underfitting since it lowers the effect of the variables' factors, hence reducing the model's intricacy.

Because of the improved accuracy of the validation data, we turned to the Adam function for optimization. After it was built, we used it to train our model. We only kept a sample that was more accurate than the previous weighing to prevent overfitting.

We resized the image to the desired size that fits our proposed system (28 x 28 x 16). Then, because Keras always requires a series of images to forecast the model, we created a batch of photographs with specified batch size. Because we're only evaluating specific images, we'll make a single-size group. Finally, we projected that the model would yield a value ranging from 0 to 7 since our model expected 7 different skin conditions.

A data augmentation strategy was utilized to reduce overtraining. We also examined the data sets with several color models to see how well they performed with various color images.

4.6.4. Model Testing

The test data is entered, preprocessed, and fed into a trained Dense CNN model during the model testing stage. The test image is processed through each layer in search of potential disease-affected traits. If it is discovered, the system produces an output verifying maliciousness based on the information gained during the training phase. If this is not the case, the system issues a benign confirmation. The output form's form is checked in two ways: 1- Check that it corresponds to the labels in our dataset. 2- Making sure that a single scalability step on a group of data minimizes loss. Figure (4.13) explain the process of testing-training the proposed model.

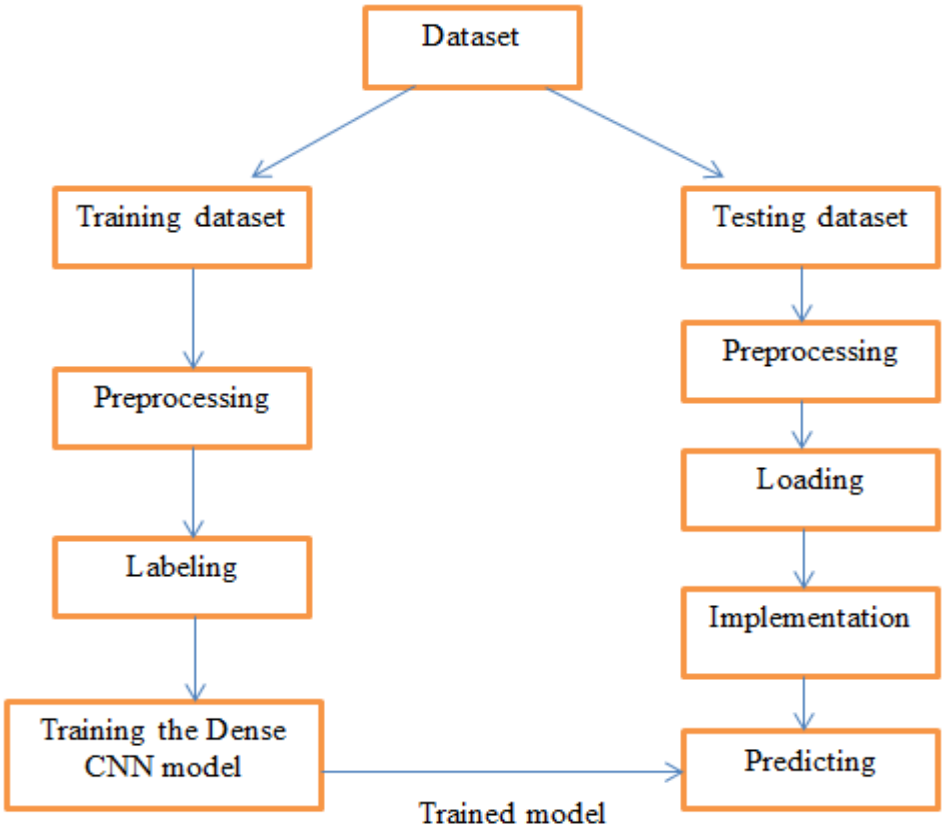

Figure 4.13. Flowchart of Testing-Training model

PART 5

RESULT AND DISCUSSION

This section presents the proposed model's results after its implementation on eight data sets. We review the results with plots of the confusion matrix, training-testing accuracy, and training-testing loss.

We divided the data set into 75 for training, 5% for validation, and 20% for testing. The accuracy, specificity, sensitivity, accuracy, and receiver operating characteristics (ROC) results were presented with a 7 x 7 noise matrix for each data set.

We review the results obtained by applying the proposed model to eight datasets (ISIC 2019, DermIS-DermQuest, HAM10000, ISIC 2017, ISIC 2016, MED-NODE, PH2 dataset, and DermNet).

Through the results, it is clear to us that our model has achieved results in accuracy, specificity, sensitivity, accuracy, and AUC much better than the results of previous studies.

The experimental results of the proposed model showed that the highest prediction accuracy was obtained by applying the model to the ISIC 2019 data set, where it was 98.06%. While the lowest prediction accuracy was 94.01% when applying our model to the MEDNODE dataset.

We will review the experimental results that we have performed on eight datasets through tables that include performance metrics, through plots that include training-testing accuracy and training-testing loss, and through the confusion matrix, which it's a metric for how well you understand categorization tasks, with the output being

two potential combinations of expected and actual values in the table. It's great for determining recall, precision, specificity, and, most crucially, the AUC-ROC curve.

Table (5.1) shows the distribution of the original number of image data for each data set, then the distribution of the data after the process of data augmentation into the test, training and verification sets.

Table 5.1. Distribution of the images after data augmentation

DATASET	NO. of ORIGIN IMAGES	NO. of AUGMEN-TED IMAGES	TRAINING IMAGES	TESTING IMAGES	VALIDA-TION IMAGES
HAM10000	10015	46935	35201	9387	2347
ISIC 2019	8520	40579	30434	8116	2029
DermIS-DermQuest	6600	30779	23084	6156	1539
ISIC 2017	6030	27986	20990	5598	1398
ISIC 2016	6400	29246	21935	5850	1461
MED-NODE	4332	20258	15194	4052	1012
PH^2 dataset	200	847	635	170	42
DermNet	571	2590	1942	518	130

5.1. TEST RESULTS OF DENSE ON HAM10000 DATASET

The application of the dense-CNN model on the HAM10000 dataset gave a prediction accuracy of 97.77 % for melanoma disease. Figure (5.1) includes plots (A and B) for training-testing accuracy and training-testing loss. Table (5.2) explains the performance metrics specificity, sensitivity, precision and AUC. Figure (5.2) displays the confusion matrix of our model on HAM10000 dataset.

Table 5.2. Performance of Dense-CNN on the HAM10000 dataset.

Dataset	Accuracy	Sensitivity	Specificity	Precision	AUC
HAM 10000	97.77 %	97.78 %	99.62 %	97.85 %	98.9 %

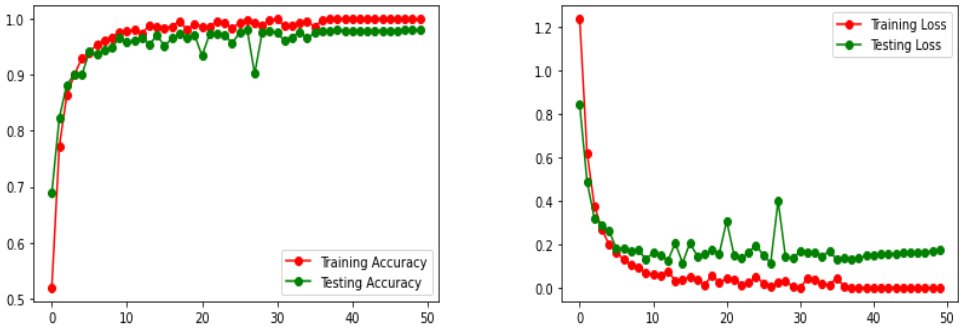

A. Training-Testing accuracy B. Training-Testing loss

Figure 5.1. Plots (A and B) show the performance results of the Dense-CNN model using the HAM 10000 dataset.

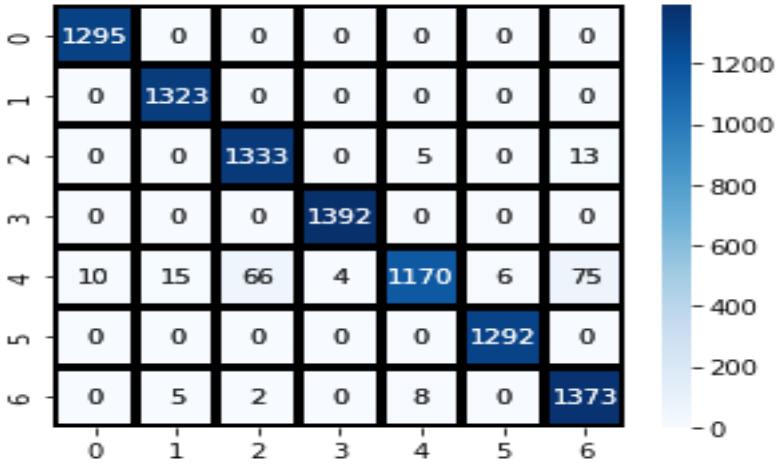

Figure 5.2. Confusion matrix for Dense-CNN with 50 epochs-9387 testing images of HAM10000 dataset.

5.2. TEST RESULTS OF DENSE ON THE ISIC 2019 DATASET

The application of the dense-CNN model on the ISIC 2019 dataset gave a prediction accuracy of 98.06% for melanoma disease. Figure (5.3) includes plots (A and B) for training-testing accuracy and training-testing loss. Table (5.3) explains the performance metrics specificity, sensitivity, precision and AUC. Figure (5.4) displays the confusion matrix of our model on ISIC 2019 dataset.

Table 5.3. Describes the performance of Dense-CNN on the ISIC 2019 dataset.

Dataset	Accuracy	Sensitivity	Specificity	Precision	AUC
ISIC 2019	98.06 %	98.07 %	99.67 %	98.13 %	99.5 %

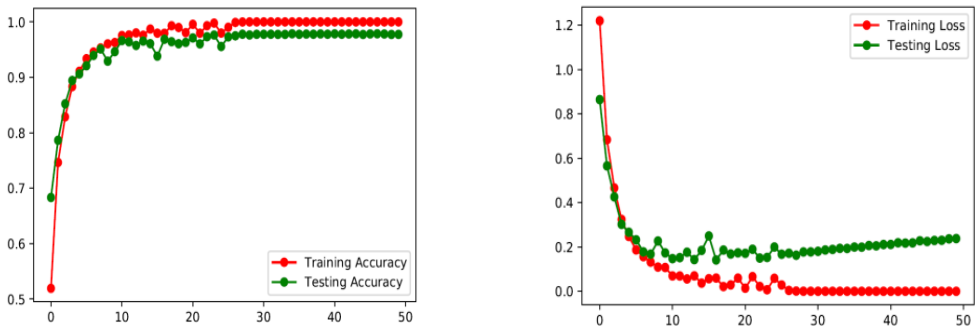

A. Training-Testing accuracy B. Training-Testing loss

Figure 5.3. Plots (A and B) show the performance results of the Dense-CNN model using the ISIC 2019 dataset.

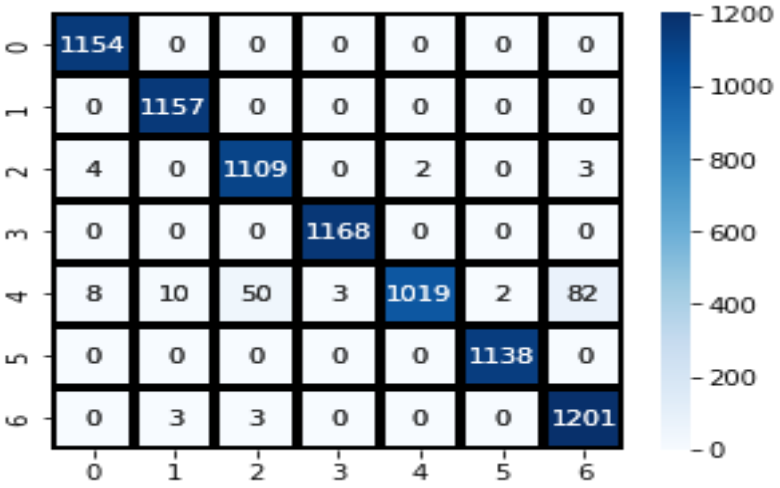

Figure 5.4. Confusion matrix for Dense-CNN model with 50 epochs-8116 testing images of ISIC 2019 dataset.

5.3. TEST RESULTS OF DENSE ON THE DERMIS DERMQUEST

The application of the dense-CNN model on the DermIS-DermQuest dataset gave a prediction accuracy of 97.85 % for melanoma disease. Figure (5.5) includes plots (A and B) for training-testing accuracy and training-testing loss. Table (5.4) explains the performance metrics specificity, sensitivity, precision and AUC. Figure (5.6) displays the confusion matrix of our model on DermIS-DermQuest dataset.

Table 5.4. Describes the performance of Dense-CNN on the DermIS-DermQuest dataset.

Dataset	Accuracy	Sensitivity		Specificity	Precision	AUC
DermIS-DermQuest	97.85 %	97.87 %		99.64 %	97.91 %	98.8 %

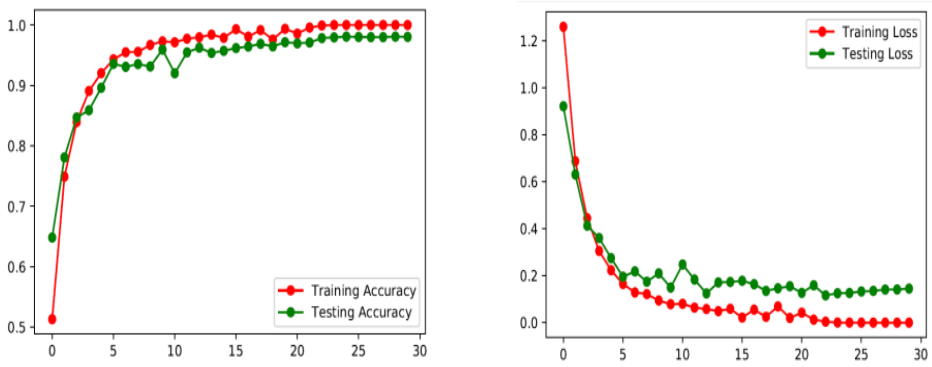

A. Training-Testing accuracy B. Training-Testing loss

Figure 5.5. Plots (A and B) show the performance results of the Dense-CNN model using the DermIS-DermQuest dataset.

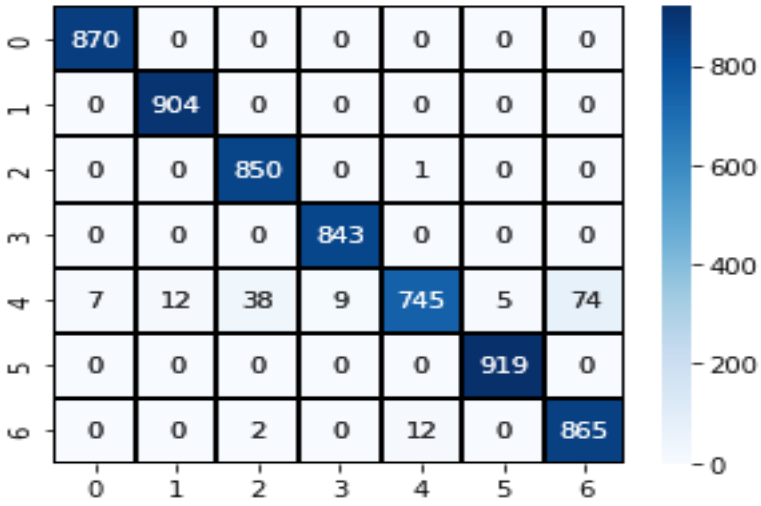

Figure 5.6. Confusion matrix for Dense-CNN model with 50 epochs- 6156 testing images of DermIS-DermQuest dataset.

5.4. TEST RESULTS OF DENSE ON THE ISIC 2017 DATASET

The application of the dense-CNN model on the ISIC 2017 dataset gave a prediction accuracy of 97.88 % for melanoma disease. Figure (5.7) includes plots (A and B) for training-testing accuracy and training-testing loss. Table (5.5) explains the performance metrics specificity, sensitivity, precision and AUC. Figure (5.8) displays the confusion matrix of our model on ISIC 2017 dataset.

Table 5.5. Describes the performance of Dense-CNN on the ISIC 2017 dataset.

Dataset	Accuracy	Sensitivity	Specificity	Precision	AUC
ISIC 2017	97.88 %	97.89 %	99.64 %	97.97 %	99.2 %

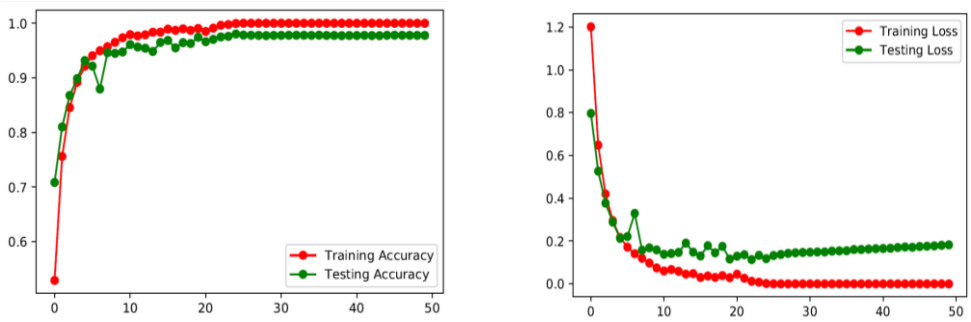

A. Training-Testing accuracy B. Training-Testing loss

Figure 5.7. Plots (A and B) show the performance results of the Dense-CNN model on the ISIC 2017 dataset.

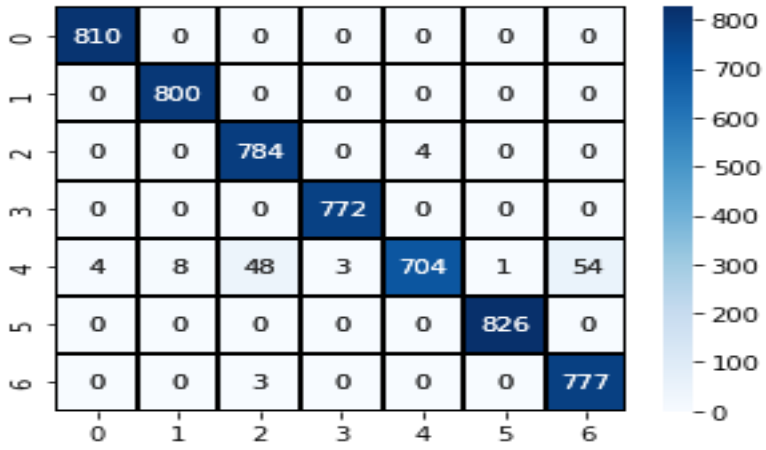

Figure 5.8. Confusion matrix for Dense-CNN with 50 epochs- 5598 testing images of ISIC 2017 dataset.

5.5. TEST RESULTS OF DENSE ON THE ISIC 2016 DATASET

The application of the dense-CNN model on the ISIC 2016 dataset gave a prediction accuracy of 94.66 % for melanoma disease. Figure (5.9) includes plots (A and B) for training-testing accuracy and training-testing loss. Table (5.6) explains the performance metrics specificity, sensitivity, precision and AUC. Figure (5.10) displays the confusion matrix of our model on ISIC 2016 dataset.

Table 5.6. Describes the performance of Dense-CNN on the ISIC 2016 dataset.

Dataset	Accuracy	Sensitivity	Specificity	Precision	AUC
ISIC 2016	94.66 %	94.72 %	99.11 %	94.66 %	96.5 %

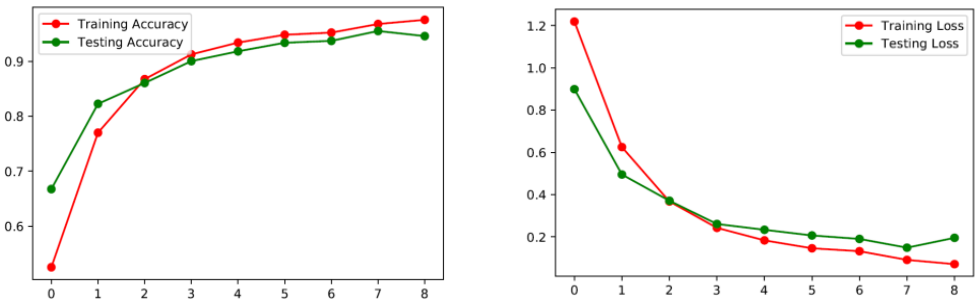

A. Training-Testing accuracy B. Training-Testing loss

Figure 5.9. Plots (A and B) show the performance results of the Dense-CNN model on the ISIC 2016 dataset.

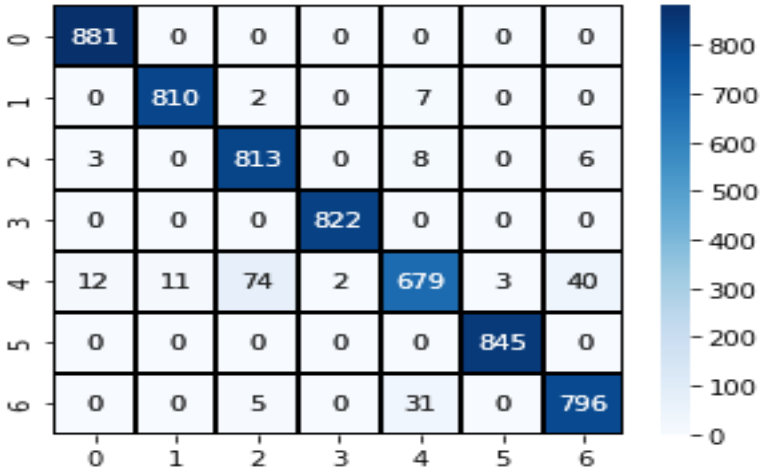

Figure 5.10 Confusion matrix for Dense-CNN with 50 epochs- 5850 testing images of ISIC 2016 dataset.

5.6. TEST RESULTS OF DENSE ON THE MED-NODE DATASET

The application of the dense-CNN model on the MED-NODE dataset gave a prediction accuracy of 94.01 % for melanoma disease. Figure (5.11) includes plots (A and B) for training-testing accuracy and training-testing loss. Table (5.7) explains the performance metrics specificity, sensitivity, precision and AUC. Figure (5.12) displays the confusion matrix of our model on MED-NODE dataset.

Table 5.7. Describes the performance of Dense-CNN on the MED-NODE dataset.

Dataset	Accuracy	Sensitivity	Specificity	Precision	AUC
MED-NODE	94.01 %	94.06 %	99. %	94.19 %	95.2 %

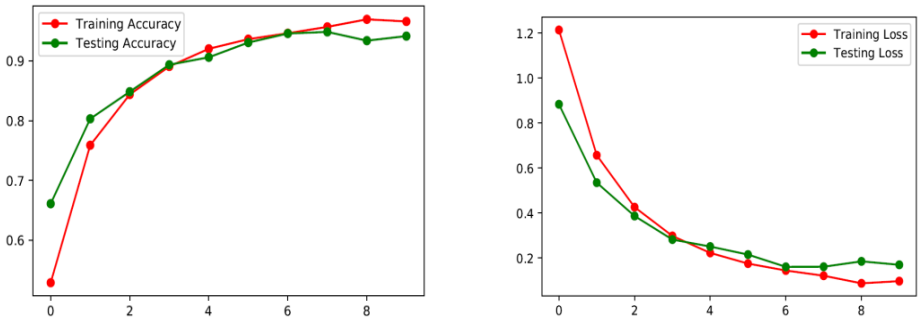

A. Training-Testing accuracy B. Training-Testing loss

Figure 5.11. Plots (A and B) show the performance results of the Dense-CNN model on the MED-NODE dataset.

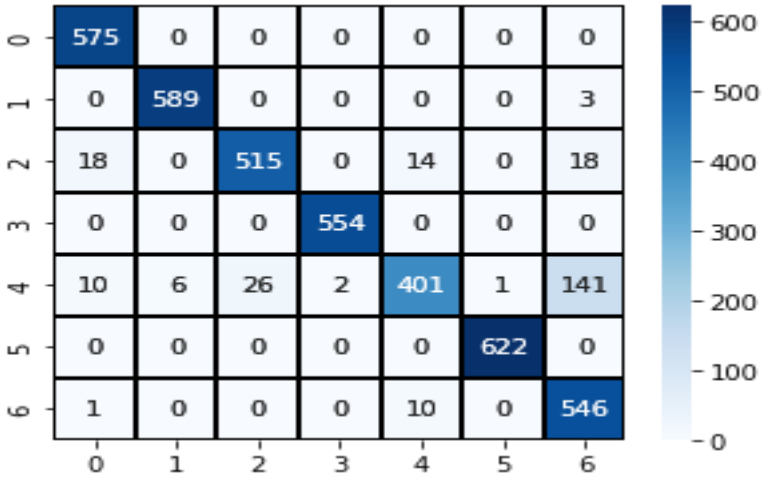

Figure 5.12. Confusion matrix for Dense-CNN with50 epochs- 4052 testing images of MED-NODE dataset.

5.7. TEST RESULTS OF DENSE ON THE PH² DATASET

The application of the dense-CNN model on the PH² dataset gave a prediction accuracy of 97.81 % for melanoma disease. Figure (5.13) includes plots (A and B) for training-testing accuracy and training-testing loss. Table (5.8) explains the performance metrics specificity, sensitivity, precision and AUC. Figure (5.14) displays the confusion matrix of our model on PH2 dataset.

Table 5.8. Describes the performance of Dense-CNN on the PH² dataset.

Dataset	Accuracy	Sensitivity	Specificity	Precision	AUC
PH² dataset	97.81 %	97.83 %	99.63%	97.87 %	98.8 %

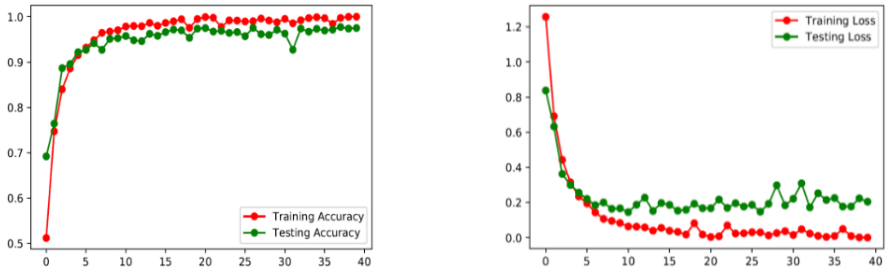

A. Training-Testing accuracy B. Training-Testing loss

Figure 5.13. Plots (A and B) show the performance results of the Dense-CNN model on the PH² dataset.

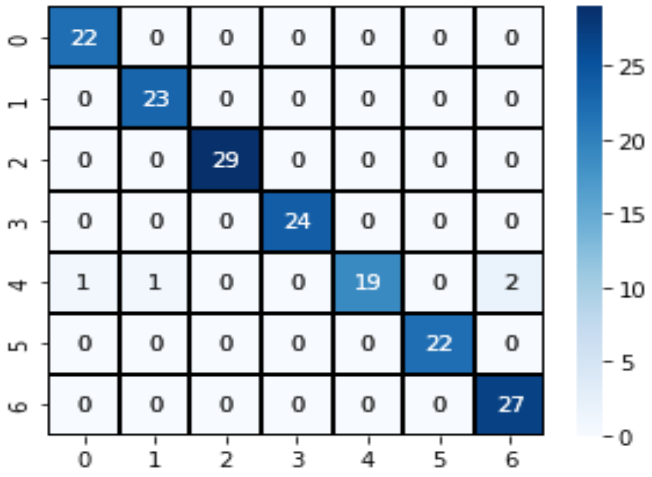

Figure 5.14. Confusion matrix for Dense-CNN with 50 epochs-170 testing images of PH² dataset.

5.8. TEST RESULTS OF DENSE ON THE DERMNET DATASET

The application of the dense-CNN model on the DermNet dataset gave a prediction accuracy of 95.46 % for melanoma disease. Figure (5.15) includes plots (A and B) for training-testing accuracy and training-testing loss. Table (5.9) explains the performance metrics specificity, sensitivity, precision and AUC. Figure (5.16) displays the confusion matrix of our model on DermNet dataset.

Table 5.9. Describes the performance of Dense-CNN on the DermNet dataset.

Dataset	Accuracy	Sensitivity	Specificity	Precision	AUC
DermNet	95.46 %	95.50 %	99.24 %	95.41 %	96.8 %

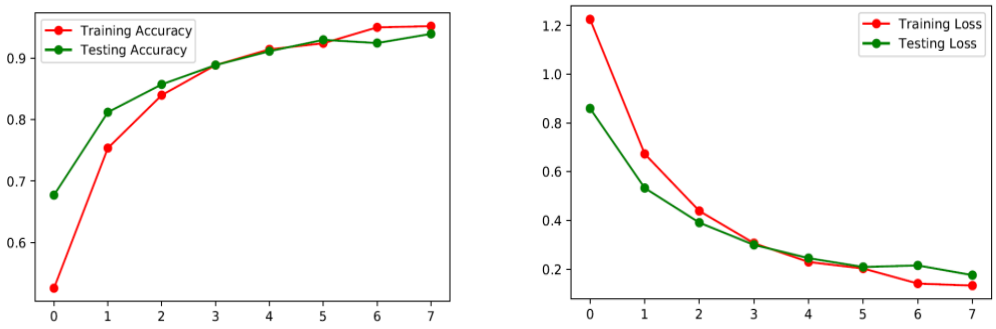

A. Training-Testing accuracy B. Training-Testing loss

Figure 5.15. Plots (A and B) show the performance results of the Dense-CNN model on the DermNet dataset.

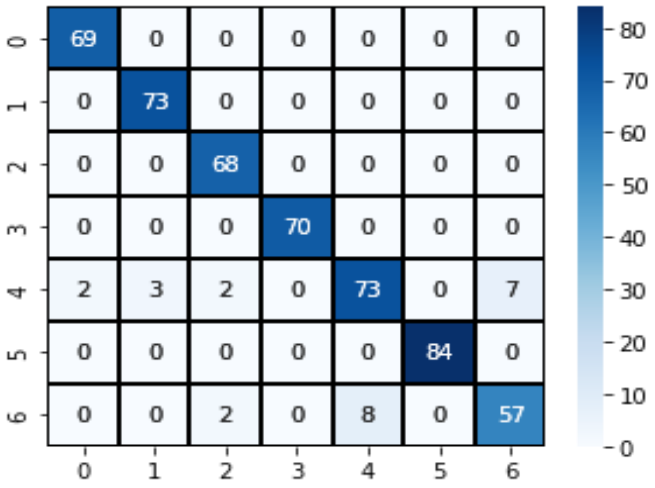

Figure 5.16. Confusion matrix for Dense-CNN with50 epochs-518 testing images of DermNet dataset.

We believe that the good results we obtained are due to several factors: 1- The strength of the model designed to contain several layers of con2D 2- The presence of three dense layers with activation functions RELU and Softmax. - Adam Enhancer was used.

4- Not using the transformed learning method because we created and trained the model. This is given that the number of epochs is 50, which serves to train the data.

In addition, we tried as much as possible to use datasets containing large numbers of skin lesion image data. Using big data allows us to get good results so that we can make comparisons with other results. Figure (5.9) shows the histogram of the accuracy results obtained by applying the proposed model to eight datasets.

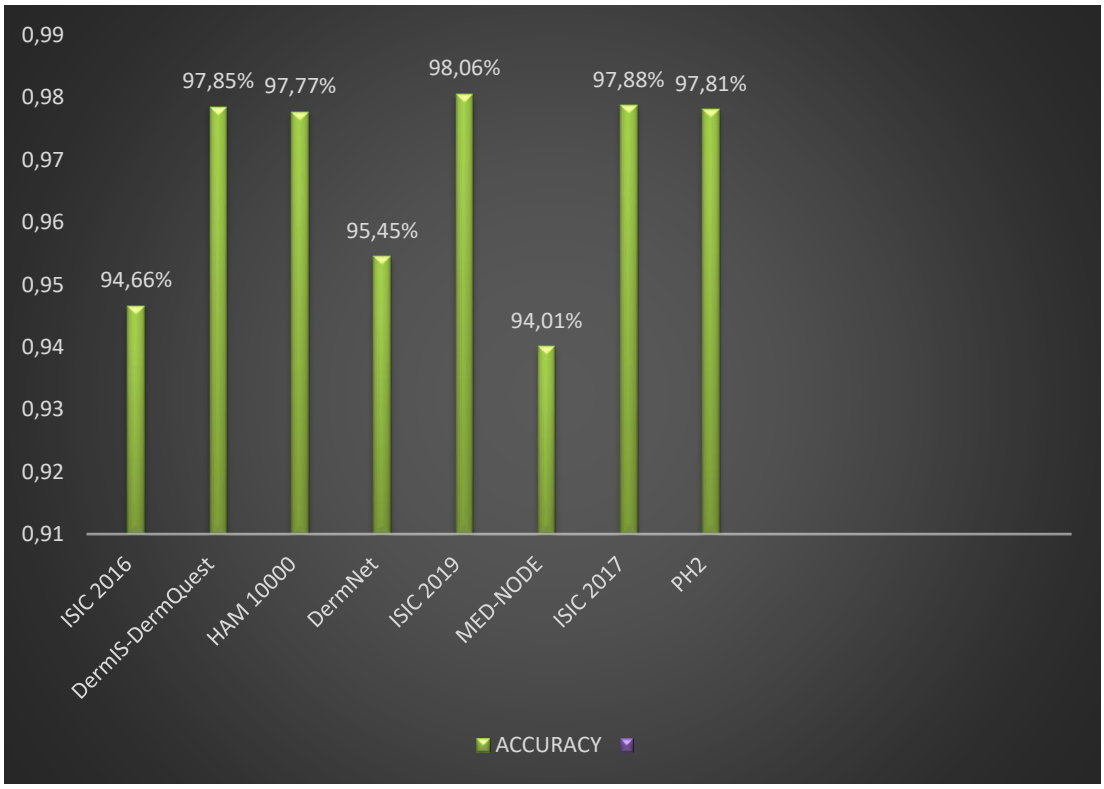

Figure 5.17. Comparison of the performance of the Dense-CNN model on eight datasets.

5.9. COMPARING WITH RELATED WORKS

From the presented results, we can say that the proposed model (Dense-CNN) has achieved very good results in diagnosing and classifying melanoma diseases, and it is possible to obtain those promising results when applied to any dataset for dermatology. According to the results for accuracy, we compared our results with other work that

used CNN in diagnosing melanoma. The comparison was the performance with the highest accuracy rate we obtained, 98.08%, when executing the model on the HAM10000 dataset. Table (5.10) shows the accuracy, sensitivity, and specificity rates we achieved compared with other methods.

Table 5.10. Comparing our experimental results with other exciting works and our proposed model (highest rate with ISIC 2019).

METHOD	ACCURACY	SENSITI-VITY	SPECIFI-CITY	PRECISION
CNN's and GANs [27]	92.4%	48.3%	97.7%	–
CNN [30]	83.07%	–	–	–
AlexNet [31]	84.4%	84.7%	83.8%	–
VGGNet [32]	81.33%	78.66%	–	–
CNN , SVM [28]	94%	100%	88%	–
ELM [34]	93%	–	–	–
DNN [43]	81.75 %	75.5 %	88 %	–
GWO-DNN [46]	87.98 %	96.78 %	76.54 %	–
FCN+CNN [97]	92%	94%	93%	–
DCNN [98]	80.5 %	72 %	89 %	–
Proposed method on ISIC2019 dataset (highest rate)	98.06 %	98.07 %	99.67 %	98.13 %

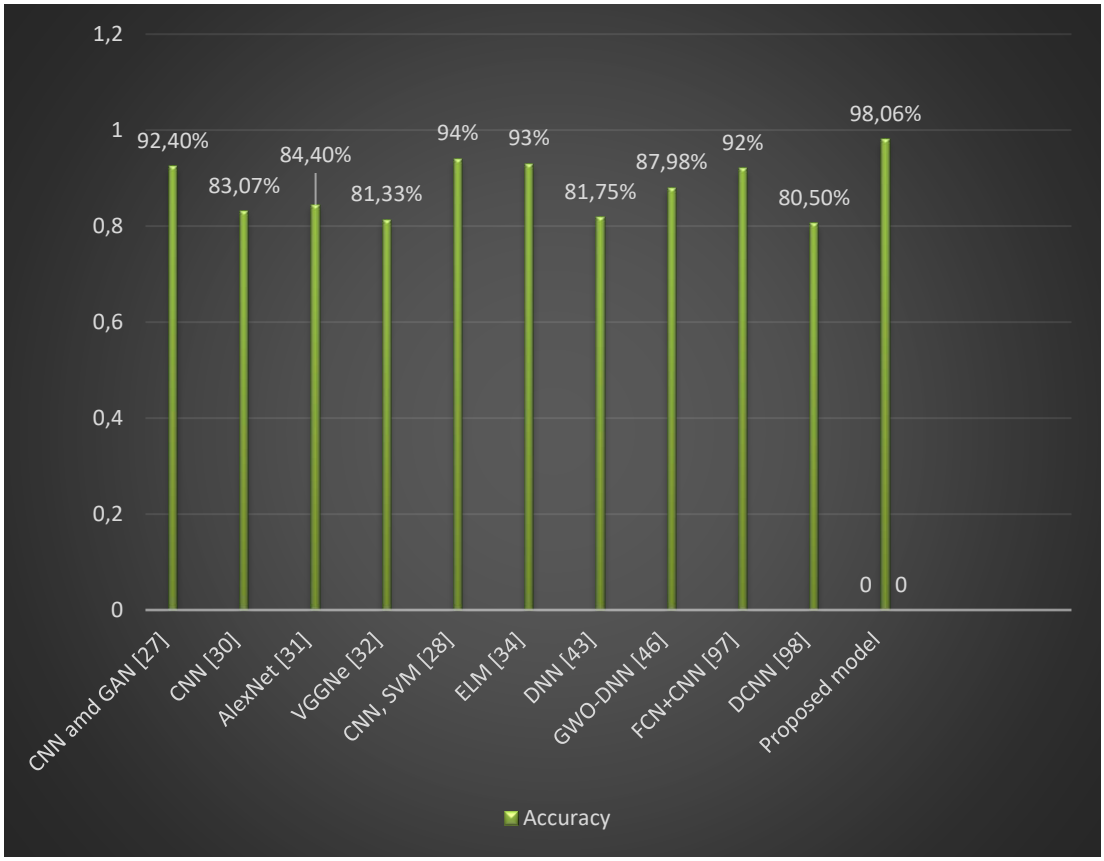

Figure 5.18. A comparison of the prediction accuracy between our proposed model (highest rate with ISIC 2019) and other existing studies.

PART 6

CONCLUSION

A new, improved technique for identifying melanoma from the input images is proposed in this work. The method was developed with the assistance of a convolutional neural network. The effectiveness of CNN may be improved with an algorithm called a dense layer. The effective approach is used to find the optimal weights and biases for the network to lessen the number of errors produced by the actual network outputs. The proposed technique successfully detected and predicted melanoma with good outcomes through thorough study and deep data comprehension.

We put the proposed method through its paces on eight different datasets (ISIC 2019, DermIS-DermQuest HAM10000, ISIC 2017, ISIC 2016, MED-NODE, PH2 dataset, and DermNet). The results we obtained indicate that the proposed technique achieved the highest accuracy of 98.06% when applied to the ISIC 2019 dataset and that the lowest accuracy achieved reached 94.01% when applied to the MED-NODE data set. The results obtained were compared with those of previous investigations, with accuracy, specificity, sensitivity, accuracy, and AUC serving as performance measures. The final results showed that the application of the proposed model had achieved the best results in diagnosing skin cancer, and this accuracy has outperformed all the results of previous studies that compared it.

For future work, we suggest dividing the major skin lesions into several subcategories to ensure the best classification of skin lesions.

REFERENCES

1. WALLINGFORD, Sarah C., et al. Skin cancer arising in scars: a systematic review. ***Dermatologic surgery***, 37.9: 1239-12 (2011).

2. Rigel, D. S., Russak, J., and Friedman, R., "The Evolution of Melanoma Diagnosis: 25 Years Beyond the ABCDs", CA: ***A Cancer Journal For Clinicians***, 60 (5): 301–316 (2010).

3. Siegal, R., Miller, K. D., and Jemal, A., "Cancer statistics, 2012", ***Ca Cancer J Clin***, 64 (1): 9–29 (2014).

4. Matheny, Israni, M. and, Ahmed, S. T. and, Whicher, M. and, and Danielle, "Artificial intelligence in health care: the hope, the hype, the promise, the peril", ***Washington, DC: National Academy Of Medicine***, (2019).

5. Brown, Kimberly M. Melanoma, "An Issue of Surgical Clinics, E-Book", Vol. 94. No. 5. ***Elsevier Health Sciences,*** (2014) .

6. Mehta, P. and Shah, B., "Review on Techniques and Steps of Computer Aided Skin Cancer Diagnosis", ***Procedia - Procedia Computer Science***, 85 (Cms): 309–316 (2016).

7. Smith, R. A., et.al, "Cancer screening in the United States, 2017: A review of current American Cancer Society guidelines and current issues in cancer screening", ***CA: A Cancer Journal For Clinicians***, 67 (2): 100–121 (2017).

8. Sagar, Abhinav, and Dheeba Jacob. "Convolutional neural networks for classifying melanoma images." ***bioRxiv*** (2021)

9. Kassem, M. A., Hosny, K. M., and Fouad, M. M., "Skin Lesions Classification Into Eight Classes for ISIC 2019 Using Deep Convolutional Neural Network and Transfer Learning", ***IEEE Access*** , 8: (2020).

10. Dubal, P., Bhatt, S., Joglekar, C., and Patil, S., "Skin Cancer Detection and Classification", ***2017 6th international conference on electrical engineering and informatics (ICEEI). IEEE,***(2017)

11. Munir, K., Elahi, H., Ayub, A., Frezza, F., and Rizzi, A., "Cancer diagnosis using deep learning: A bibliographic review", ***Cancers***, 11 (9): (2019).

12. Abbas, Q. and Celebi, M. E., "DermoDeep-A classification of melanoma-nevus skin lesions using multi-feature fusion of visual features and deep neural network", ***Multimedia Tools And Applications*** 2019 78:16, 78 (16): 23559–23580 (2019).

13. Khan, M. Q., Hussain, A., Rehman, S. U. R., and Khan, U., "Classification of Melanoma and Nevus in Digital Images for Diagnosis of Skin Cancer", ***IEEE Access***, 7: 90132–90144 (2019).

14. Garg, Rishu, Saumil Maheshwari, and Anupam Shukla. "Decision support system for detection and classification of skin cancer using CNN." ***Innovations in Computational Intelligence and Computer Vision. Springer, Singapore***, (2021).

15. Doi, K., "Computer-aided diagnosis in medical imaging: Historical review, current status and future potential", ***Computerized Medical Imaging And Graphics,*** 31 (4–5): 198–211 (2007).

16. Eadie, L. H., Taylor, P., and Gibson, A. P., "A systematic review of computer-assisted diagnosis in diagnostic cancer imaging", ***European Journal Of Radiology***, 81 (1): e70–e76 (2012).

17. Doi, K., "Current status and future potential of computer-aided diagnosis in medical imaging", ***British Journal Of Radiology***, 78 (SPEC. ISS.): 21–30 (2005).

18. Ahnlide, I., Bjellerup, M., Nilsson, F., and Nielsen, K., "Validity of ABCD rule of dermoscopy in clinical practice", ***Acta Dermato-Venereologica***, 96 (3): 367–373 (2016).

19. Capdehourat, G., Corez, A., Bazzano, A., Alonso, R., and Musé, P., "Toward a combined tool to assist dermatologists in melanoma detection from dermoscopic images of pigmented skin lesions", ***Pattern Recognition Letters,*** 32 (16): 2187–2196 (2011).

20. Iqtidar, K., Aziz, S., and Khan, M. U., "Image Pattern Analysis towards Classification of Skin Cancer through Dermoscopic Images", ***First International Conference of Smart Systems and Emerging Technologies (SMARTTECH). IEEE1–7*** (2020).

21. Adler, Nikki R., et al. "Methods of melanoma detection and of skin monitoring for individuals at high risk of melanoma: new Australian clinical practice." ***Medical Journal of Australia*** 210.1 (2019)

22. Leo, G. Di, Paolillo, A., and Sommella, P., "Automatic Diagnosis of Melanoma Based on the 7-Point Checklist Automatic Diagnosis of Melanoma : a Software System based on the 7-Point", ***Hawaii international conference on system sciences. IEEE***, (2014).

23. Sadeghi, M., "Towards prevention and early diagnosis of skin cancer : computer-aided analysis of dermoscopy images", ***(Doctoral dissertation, Applied Science: School of Computing Science)***, (2012).

24. Pham, T. C., Tran, G. S., Nghiem, T. P., Doucet, A., Pham, T. C., Tran, G. S., Nghiem, T. P., Doucet, A., Luong, C. M., and Doucet, A., "A Comparative Study for Classification of Skin Cancer To cite this version : HAL Id : hal-03025957 A comparative study for classification of skin cancer", ***Computers*** 11.5,(2020).

25. Naidu, K., Ali, M. S., Abu Bakar, A. H., Tan, C. K., Arof, H., and Mokhlis, H., "Optimized artificial neural network to improve the accuracy of estimated fault impedances and distances for underground distribution system", Plos One, 15 (1): e0227494 (2020).

26. Molina-Molina, E. O., Solorza-Calderón, S., and Álvarez-Borrego, J., "Classification of dermoscopy skin lesion color-images using fractal-deep learning features", ***Applied Sciences***, 10 (17): 5954 (2020).

27. Gong, An, Xinjie Yao, and Wei Lin. "Classification for dermoscopy images using convolutional neural networks based on the ensemble of individual advantage and group decision." ***IEEE Access*** 8 (2020).

28. Shoieb, D. A., Youssef, S. M., and Aly, W. M., "Computer-aided model for skin diagnosis using deep learning", ***Journal Of Image And Graphics,*** 4 (2): 122–129 (2016).

29. Mohamed, A., Mohamed, W., and Zekry, A. H., "Deep learning can improve early skin cancer detection", ***International Journal Of Electronics And Telecommunications***, 65 (3): 507–513 (2019).

30. Mukherjee, S., Adhikari, A., and Roy, M., "Malignant Melanoma Classification Using Cross-Platform Dataset with Deep Learning CNN Architecture", ***Advances In Intelligent Systems And Computing***, 922: 31–41 (2019).

31. Kaymak, S., Esmaili, P., and Serener, A., "Deep Learning for Two-Step Classification of Malignant Pigmented Skin Lesions", 2018 14th ***Symposium On Neural Networks And Applications, NEUREL , IEEE,*** 2018, 1–6 (2018).

32. Lopez, Adria Romero, et al. "Skin lesion classification from dermoscopic images using deep learning techniques." 2017 13th ***IASTED international conference on biomedical engineering (BioMed). IEEE***, (2017).

33. Albahar, Marwan Ali. "Skin lesion classification using convolutional neural network with novel regularizer." ***IEEE Access*** 7, (2019).

34. Nida, N., Irtaza, A., and Yousaf, M. H., "A Novel Region-Extreme Convolutional Neural Network for Melanoma Malignancy Recognition", ***Mathematical Problems in Engineering***, (2021).

35. Kanimozhi, T. and Murthi, A., "Computer aided Melanoma skin cancer detection using Artificial Neural Network classifier", ***Singaporean Journal Of Scientific Research(SJSR) Journal Of Selected Areas InMicroelectronics (JSAM)***, 8 (2): 35–42 (2016).

36. Dalila, F., Zohra, A., Reda, K. and Hocine, C., "Segmentation and classification of melanoma and benign skin lesions." ***Optik*** 140, (2017).

37. Sugiarti, S., Yuhandri, Y., Na'am, J., Indra, D. and Santony, J., "An artificial neural network approach for detecting skin cancer." ***TELKOMNIKA (Telecommunication Computing Electronics and Control)*** 17.2 ,(2019) .

38. Majumder, S., Ullah, M. A., and Dhar, J. P., "Melanoma Diagnosis from Dermoscopy Images Using Artificial Neural Network", ***International Conference on Advances in Electrical Engineering (ICAEE). IEEE*** , (2019).

39. Elgamal, M., "Automatic Skin Cancer Images Classification", ***International Journal Of Advanced Computer Science And Applications***, 4 (3): (2013).

40. Ding, Y., Smith, L., Smith, M., Sun, J., and Warr, R., "A computer assisted diagnosis system for malignant melanoma using 3D skin surface texture features and artificial neural network", ***International Journal Of Modelling, Identification And Control***, 9 (4): 370–381 (2010).

41. Li, L., Zhang, Q., Ding, Y., Jiang, H., Thiers, B. H., and Wang, J. Z., "Automatic diagnosis of melanoma using machine learning methods on a spectroscopic system", ***BMC Medical Imaging***, 14 (1): 1–12 (2014).

42. Zhang, N., Cai, Y. X., Wang, Y. Y., Tian, Y. T., Wang, X. L., and Badami, B., "Skin cancer diagnosis based on optimized convolutional neural network", ***Artificial Intelligence In Medicine***, 102: 101756 (2020).

43. Chandra, T. G., Nasution, A. M. T., and Setiadi, I. C., "Melanoma and nevus classification based on asymmetry, border, color, and GLCM texture parameters using deep learning algorithm", ***AIP Conference Proceedings***, 2193 (December): (2019).

44. Abbes, W. and Sellami, D., "Deep neural network for fuzzy automatic melanoma diagnosis", VISIGRAPP 2019 - Proceedings Of The 14th ***International Joint Conference On Computer Vision, Imaging And Computer Graphics Theory And Applications, 4 (Visigrapp)***: 47–56 (2019).

45. Maiti, A. and Chatterjee, B., "Improving detection of Melanoma and Naevus with deep neural networks", ***Multimedia Tools And Applications***, 79 (21–22): 15635–15654 (2020).

46. Daniel, A., et al. "IoT-Based Automated Skin Lesion Detection and Classification Using Gray Wolf Optimization with Deep Neural Network." ***Artificial Intelligence Techniques in IoT Sensor Networks. Chapman and Hall/CRC***, 197-212, (2020).

47. Zadeh Shirazi, A. and Mohammadi, Z., "A hybrid intelligent model combining ANN and imperialist competitive algorithm for prediction of corrosion rate in 3C steel under seawater environment", ***Neural Computing And Applications***, 28 (11): 3455–3464 (2017).

48. Jankowski, Norbert, and Marek Grochowski. "Comparison of instances seletion algorithms i. algorithms survey." ***International conference on artificial intelligence and soft computing*. Springer, Berlin, Heidelberg**, (2004).

49. Mahesh, Batta. "Machine learning algorithms-a review." ***International Journal of Science and Research (IJSR).[Internet]*** 9: 381-386. (2020)

50. Prakash, V. J. and Nithya, D. L. M., "A Survey On Semi-Supervised Learning Techniques", ***International Journal Of Computer Trends And Technology***, 8 (1): 25–29 (2014).

51. Berry, Michael W., Azlinah Mohamed, and Bee Wah Yap, eds. Supervised and unsupervised learning for data science. ***Springer Nature***, (2019).

52. Carlini, Nicholas. "Poisoning the Unlabeled Dataset of {Semi-Supervised} Learning." 30th ***USENIX Security Symposium (USENIX Security 21)***. (2021).

53. Mousavi, Seyed Sajad, Michael Schukat, and Enda Howley. "Deep reinforcement learning: an overview." ***Proceedings of SAI Intelligent Systems Conference*. Springer, Cham,** (2016).

54. Li, Hongfeng, et al. "Skin disease diagnosis with deep learning: a review." ***Neurocomputing*** 464: 364-393, (2021)..

55. Mirunalini, P., Chandrabose, A., Gokul, V., and Jaisakthi, S. M., "Deep learning for skin lesion classification", ***ArXiv Preprint ArXiv***:1703.04364, (2017).

56. Krizhevsky, A., Sutskever, I. and Hinton, G.E,. "Imagenet classification with deep convolutional neural networks." ***Advances in neural information processing systems*** 25 (2012).

57. Kim, K.G., "Book review: Deep learning." ***Healthcare informatics research*** 22.4 (2016).

58. Smirnov, E. A., Timoshenko, D. M., and Andrianov, S. N., "Comparison of Regularization Methods for ImageNet Classification with Deep Convolutional Neural Networks", ***AASRI Procedia***, 6: 89–94 (2014).

59. Zhou, Jie, et al. "Deep recurrent models with fast-forward connections for neural machine translation." ***Transactions of the Association for Computational Linguistics*** 4-371-383, (2016).

60. Afouras, T., Chung, J.S., Senior, A., Vinyals, O. and Zisserman, A,. "Deep audio-visual speech recognition." ***IEEE transactions on pattern analysis and machine intelligence*** ,(2018).

61. Wang, Z. J., Turko, R., Shaikh, O., Park, H., Das, N., Hohman, F., Kahng, M., and Chau, D. H. P., "Cnn explainer: Learning convolutional neural networks with interactive visualization", ***IEEE Transactions On Visualization And Computer Graphics,*** 27 (2): 1396–1406 (2020).

62. Sewak, M., Karim, M. R., and Pujari, P., "Practical Convolutional Neural Networks: Implement Advanced Deep Learning Models Using Python", ***Packt Publishing Ltd***, (2018).

63. Rasul, M. F., Dey, N. K., and Hashem, M. M. A., "A Comparative Study of Neural Network Architectures for Lesion Segmentation and Melanoma Detection", 2020 Region 10 ***Symposium, TENSYMP, IEEE***, 2020, (June): 1572–1575 (2020).

64. Li, Q., Cai, W., Wang, X., Zhou, Y., Feng, D.D. and Chen, M., "Medical image classification with convolutional neural network." 2014 13th ***international conference on control automation robotics & vision (ICARCV). IEEE***, (2014).

65. Vedaldi, Andrea, and Karel Lenc. "Matconvnet: Convolutional neural networks for matlab." Proceedings of the 23rd ***ACM international conference on Multimedia***. (2015).

66. Kuo, C.-C. J., "Understanding convolutional neural networks with a mathematical model", ***Journal Of Visual Communication And Image Representation***, 41: 406–413 (2016).

67. Nwankpa, C., Ijomah, W., Gachagan, A., and Marshall, S., "Activation Functions: Comparison of trends in Practice and Research for Deep Learning", ***arXiv preprint arXiv****:1811.03378* ,1–20 (2018).

68. Hara, K., "Analysis of Function of Rectified Linear Unit Used in Deep learning", ***international joint conference on neural networks (IJCNN). IEEE***, (March 2018): (2015).

69. Rawat, W. and Wang, Z., "Deep Convolutional Neural Networks for Image Classification : A Comprehensive Review Deep Convolutional Neural Networks for Image Classification : A Comprehensive Review", ***Neural computation*** 29.9 (2017): (2017).

70. Fritz, M., "Learnable Pooling Regions for Image Classification", ***arXiv preprint arXiv****:1301.3516* 1–10 (2009).

71. O'Shea, K. and Nash, R., "An Introduction to Convolutional Neural Networks", ***arXiv preprint arXiv****:1511.08458* , 1–11 (2015).

72. Basha, S.S., Dubey, S.R., Pulabaigari, V. and Mukherjee, S., "Impact of fully connected layers on performance of convolutional neural networks for image classification." ***Neurocomputing*** 378 (2020).

73. Shelhamer, E., Long, J. and Darrell, T.,"Fully convolutional networks for semantic segmentation." ***IEEE transactions on pattern analysis and machine intelligence*** 39.4 (2016).

74. Garbin, C., Zhu, X., and Marques, O., "Dropout vs . batch normalization : an empirical study of their impact to deep learning", ***Multimedia Tools and Applications*** 79.19,12777-12815,(2020).

75. Chang, C., Rampasek, L., and Goldenberg, A., "Dropout Feature Ranking for Deep Learning Models", ***arXiv preprint arXiv****:1712.08645*,(2018).

76. Achille, A. and Soatto, S., "Information Dropout : Learning Optimal Representations Through Noisy Computation", ***IEEE Transactions On Pattern Analysis And Machine Intelligence***, 40 (12): 2897–2905 (2018).

77. Huang, G., Liu, Z., Van Der Maaten, L. and Weinberger, K.Q., "Densely connected convolutional networks." ***Proceedings of the IEEE conference on computer vision and pattern recognition***,(2017).

78. Waheed, et al. "An optimized dense convolutional neural network model for disease recognition and classification in corn leaf." ***Computers and Electronics in Agriculture*** 175 (2020).

79. Huang, G., Li, T., and Wu, F., "Multi-Scale Dense Convolutional Networks for Efficient Prediction", ***arXiv preprint arXiv****:1703.09844* 2, (2017).

80. Rubin, J., Parvaneh, S., Rahman, A., Conroy, B., and Babaeizadeh, S., "Densely Connected Convolutional Networks and Signal Quality Analysis to Detect Atrial Fibrillation Using Short Single-Lead ECG Recordings",***Computing in cardiology (cinc). IEEE***, 2–5 (2017).

81. Pelt, M. and Sethian, J. A., "A mixed-scale dense convolutional neural network for image analysis", ***Proceedings of the National Academy of Sciences*** 115.2: 254-259, (2018).

82. Sutskever, I., Martens, J., Dahl, G., and Hinton, G., "On the importance of initialization and momentum in deep learning": ***In International conference on machine learning,*** pp. 1139-1147. PMLR (2013).

83. Saez, A., Acha, B., and Serrano, C., "Pattern analysis in dermoscopic images", Computer Vision Techniques for the Diagnosis of Skin Cancer, pp. 23-48. ***Springer, Berlin, Heidelberg***,, 23–48 (2014).

84. Deng, Li, Yu, and Dong, "Deep learning: methods and applications", ***Foundations And Trends In Signal Processing***, 7: 197--387 (2014).

85. Rezvantalab, A., Safigholi, H., and Karimijeshni, S., "Dermatologist Level Dermoscopy Skin Cancer Classification Using Different Deep Learning Convolutional Neural Networks Algorithms", ***arXiv preprint arXiv****:1810.10348* (2018).

86. Meyer, A., Zverinski, D., Pfahringer, B., Kempfert, J., Kuehne, T., Sündermann, S. H., Stamm, C., Hofmann, T., Falk, V., and Eickhoff, C., "Machine learning for real-time prediction of complications in critical care: a retrospective study", ***The Lancet Respiratory Medicine***, 6 (12): 905–914 (2018).

87. Fawcett, T., "An introduction to ROC analysis", ***Pattern Recognition Letters***, 27 (8): 861–874 (2006).

88. Moolayil, J., "Learn Keras for Deep Neural Networks", Learn Keras for Deep Neural Networks, ***Birmingham: Apress*** , (2019).

89. Smedley, Nova Fujuan. Learning Radiogenomic and Longitudinal Patterns to Characterize Disease Trajectory. ***University of California, Los Angeles***, 2019.

90. Barupal, D. K. and Fiehn, O., "Generating the blood exposome database using a comprehensive text mining and database fusion approach", ***Environmental Health Perspectives***, 127 (9): 2825–2830 (2019).

91. Stevens, E., Antiga, L. and Viehmann, T., "Deep learning with PyTorch", ***Manning Publications***, (2020).

92. Bergstra, J., Bastien, F., Breuleux, O., Lamblin, P., Pascanu, R., Delalleau, O., Desjardins, G., Warde-Farley, D., Goodfellow, I., Bergeron, A., and Bengio, Y., "Theano: Deep Learning on GPUs with Python", ***Journal Of Machine Learning Research***, 1: 1–48 (2011).

93. Coelho, L.P. and Richert, W., Building machine learning systems with Python. ***Packt Publishing Ltd***, (2015).

94. Gong, A., Yao, X., and Lin, W., "Classification for Dermoscopy Images Using Convolutional Neural Networks Based on the Ensemble of Individual Advantage and Group Decision", ***IEEE Access***, 8: 155337–155351 (2020).

95. Sow, B., Mukhtar, H., Ahmad, H. F., and Suguri, H., "Assessing the relative importance of social determinants of health in malaria and anemia classification based on machine learning techniques", ***Informatics For Health And Social Care***, 45 (3): 229–241 (2020).

96. Li, Y. and Shen, L., "Skin lesion analysis towards melanoma detection using deep learning network", ***Sensors (Switzerland)***, 18 (2): (2018).

97. Naeem, A., Farooq, M.S., Khelifi, A. and Abid, A., "Malignant melanoma classification using deep learning: datasets, performance measurements, challenges and opportunities." ***IEEE Access*** 8 (2020)..

98. Jianu, S.R.S., Ichim, L. and Popescu, D, "Automatic diagnosis of skin cancer using neural networks." 2019 11th ***International Symposium on Advanced Topics in Electrical Engineering (ATEE). IEEE*** (2019).

RESUME

Mohammed Yousif Arabi graduated from primary education in Iraq's Nasiriyah. He completed his secondary education in the province of Thi-Qar, then obtained a bachelor's degree from Al-Imam Al-Kadhim University for Islamic Sciences/Dhi Qar-Department of Computer Engineering Techniques in 2019. After graduation, I worked briefly with the United Nations Program as a field observer. For a master's degree. In 2020 he moved to Turkey to study a master's in Karabuk, university Department of Computer Engineering.